New particle-dependent parameterizations of heterogeneous freezing processes: Sensitivity studies of convective clouds with an air parcel model.

K. Diehl[1] and S.K. Mitra[1]

[1]{Institute of Atmospheric Physics, University of Mainz, Germany}

Correspondence to: K. Diehl (kdiehl@uni-mainz.de)

Abstract

Based on the outcome of laboratory results, new particle-dependent parameterizations of heterogeneous freezing were derived and used to improve and extend a two-dimensional spectral microphysics scheme. They include (1) a particle-type dependent parameterization of immersion freezing using the numbers of active sites per mass, (2) a particle-type and size-resolved parameterization of contact freezing, and (3) a particle-type dependent description of deposition freezing. The modified microphysical scheme was embedded in an adiabatic air parcel model with entrainment. Sensitivity studies were performed to simulate convective situations and to investigate the impact of ice nuclei concentrations and types on ice formation. As a central diagnostic parameter the ice water fraction *IWF* was selected which is the relation of the ice water content to the total amount of water in condensed form. The following parameters were varied: initial aerosol particle number size distributions, types of ice nucleating particles, final temperature, and the fractions of potential ice nucleating particles. Single and coupled freezing processes were investigated. The results show that immersion freezing seems to be the most efficient process. Contact freezing is constrained by the collision kernel between supercooled drops and potential ice nucleating particles. The importance of deposition freezing lies in secondary ice formation, i.e. small ice particles produced by deposition nucleation trigger the freezing of supercooled drops by collisions. Thus, a broader ice particle spectrum is generated than by immersion and contact freezing. During coupled immersion/contact and contact/deposition freezing no competition was observed; both processes contribute to cloud ice formation but do not impede each other. As already suggested in the

literature, mineral dust particles seem to be the most important ice nucleating particles. Biological particles are probably not involved in significant ice formation. The sensitive parameters affecting cloud properties are temperature, aerosol particle composition and concentration, and particle size distribution.

1 Introduction

The importance of the ice phase in mixed-phase convective clouds is indisputable. The additional release of the latent heat of freezing enforces not only the strength of the convection; the presence of ice particles in the cloud also substantially modifies the dynamical structure and the amount of precipitation (e.g., Gilmore et al., 2004). Hence, studying the ice phase in convective mixed-phase clouds is highly relevant for the understanding of such clouds and their atmospheric impact. With the convective updraft water drops are transported into regions where the temperature is low enough to allow them to freeze. Homogeneous freezing (i.e., freezing that does not require the presence of ice nuclei) becomes efficient at temperatures below -35°C (Pruppacher and Klett, 2010). Thus, at warmer temperatures in the troposphere heterogeneous freezing (which involves ice nucleating particles) is the only process of ice initiation, potentially triggering secondary ice formation. Heterogeneous freezing significantly changes the availability of liquid water in the upper parts of the cloud since ice particles grow at the expense of liquid drops by the deposition of water vapor (Bergeron-Findeisen process) and by riming (i.e., collection of liquid water). Thus, the number of ice nucleating particles and their efficiency to initiate ice formation at temperatures above the level of homogeneous freezing determines the nature of convective clouds as it modifies cloud microphysical processes and cloud development (e.g., van den Heever et al., 2006; Ekman et al., 2007; Phillips et al., 2007; Lee et al., 2009).

For detailed investigations of cloud microphysical processes adiabatic parcel models with entrainment are often employed (e.g., Simmel et al., 2005; Leroy et al., 2006; Diehl et al., 2006; Diehl et al., 2010; Ervens and Feingold, 2012). Air parcel models describe a rising bubble of air whose volume increases with height. The advantage of parcel models is that they allow a detailed description of the cloud microphysical processes, usually achieved by the use of spectral bin-microphysical models that explicitly solve the microphysical equations (see Khain et al., 2000, for an overview).

The initiation of the ice phase in numerical models is always parameterized. As the ability of atmospheric particles to serve as ice nuclei varies over a wide temperature range for each freezing process (Pruppacher and Klett, 2010), for particular model simulations parameterizations are required which describe the effects of different types of ice nuclei. Model investigations which compared the effects of different ice nucleation schemes (Fan et al., 2010; Kulkarni et al., 2012; Ervens and Feingold, 2013) imply that cloud properties are sensitive to the surface properties of ice nucleating particles. In those studies particle surface properties were described by the contact angle Θ. Other parameterizations were related directly to different particle types and model studies showed that certain aerosol types significantly alter cloud microphysics (Diehl et al., 2006; Lohmann and Diehl, 2006; Phillips et al., 2008; Hoose et al., 2008, Storelvmo et al., 2008; Lee et al., 2008). They also allow to simulate the effects of particular aerosols such as biomass burning particles (Diehl et al., 2007), biological particles (Phillips et al., 2009), bacteria (Diehl et al., 2010), or mineral dust (DeMott et al., 2015; Hande et al., 2014).

The present investigations are part of the German Science foundation (DFG) research group INUIT (**I**ce **N**uclei Research **U**n**IT**) which was established to study heterogeneous ice formation in the atmosphere. In laboratory and field studies the number concentrations, chemical composition, surface properties and sources of atmospherically relevant ice nuclei are investigated in different freezing modes. As an outcome of these experiments, joint parameterizations are derived to be fed into a cloud model to simulate mixed-phase cloud microphysics and to quantify the contribution of ice nuclei particle types and freezing modes. For more details see the INUIT website: www.ice-nuclei.de.

One of the models employed during INUIT is an adiabatic air parcel model with entrainment and a detailed sectional description of the cloud microphysics. It describes immersion and contact freezing for various ice nuclei types such as mineral dust, soot, and biological particles (Diehl and Wurzler, 2004; Diehl et al., 2006). Deposition ice nucleation had not been included so far as it has been supposed to be of less importance for ice formation in convective clouds. It might be negligible in mixed phase clouds because water saturation is reached in the updraft after short times (e.g., Ansmann et al., 2008, based on LIDAR observations). However, the formation of only a comparably small amount of ice (initiated by few very efficient ice nuclei) might result in secondary ice nucleation with highly complex interactions and consequences. The present version of the model was improved in the way that now it contains

all heterogeneous freezing processes (deposition, contact, coupled condensation/immersion). This allows to investigate the competition of the freezing modes to understand the importance of deposition freezing in comparison to immersion and contact freezing. The effects of various ice nucleating particles were compared to each other, also considering the different freezing modes, to estimate their importance.

2 Model description

The impact of ice nucleating particles on mixed-phase convective clouds is investigated with a microphysical scheme embedded in an air parcel model with entrainment. The previous version of Diehl et al. (2006) was further developed in the way that new parameterizations were added or existing ones were modified or completely replaced.

The model of Diehl et al. (2006) contains a two-dimensional spectral microphysics scheme which divides the hydrometeor spectra into size bins (Simmel and Wurzler, 2006). These describe the number and mass of the drops or ice particles within the corresponding size range. A fixed bin structure is used combining the wetted aerosol particles and the drops in one spectrum where the soluble and total mass of aerosol particles is explicitly considered in every bin. An initial dry aerosol particle number size distribution is given where the particles are internally mixed with variable insoluble and soluble fractions. After starting the rise of the air parcel, the particles grow into the droplet part of the spectrum by condensation. The size spectra are allowed to evolve freely, they are not constrained by an underlying distribution function.

Two-dimensional means here that the microphysics is not a function of the drop size only (one-dimensional case) but a function of both drop and aerosol particle size (Simmel and Wurzler, 2006). In the one-dimensional case, equally sized drops contain only equally sized particles which affects that drops of the same sizes freeze at the same temperature (Diehl and Wurzler, 2004). However, in real clouds equally sized drops contain differently sized particles which affect the freezing temperature of the drops. The soluble parts of the aerosol particles might lead to a freezing point depression (Koop et al., 2000; Diehl and Wurzler, 2004) while the insoluble fractions might give higher freezing temperatures via immersion freezing (see Section 2.1). Thus, the two-dimensional description of the microphysics allows that drops of the same sizes freeze at different temperatures which reflects drop freezing in atmospheric clouds in a more realistic way. It is divided into 90 categories for the particulate mass and into 66 categories for the water mass, both starting with 0.002 μm in diameter, with a mass dou-

bling in every category for the water mass and a mass doubling in every other category for the particulate mass. This combination is recommended in Simmel and Wurzler (2006).

The warm microphysical processes include growth of particles and drops by water vapour deposition, shrinking of particles and drops by evaporation, collision and coalescence, and impaction scavenging of particles. The entrainment of aerosol particles, drops, ice particles, temperature, and humidity is embedded (Simmel et al., 2005). The cold cloud microphysics describes immersion and contact freezing in parameterized form for various particle types (Diehl and Wurzler, 2004; Diehl et al., 2006). Condensation freezing is included implicitly in immersion freezing. Drops which are nucleated during the ascent of the air parcel by aerosol particles entrained above the freezing level could freeze immediately by immersion freezing. The growth of ice particles by water vapour diffusion and by riming (collision with supercooled droplets) is considered. Ice particles are sampled in a second spectrum which shows the same bins as the aerosol particle/liquid drop spectrum. Once drops are frozen or particles are involved in contact or deposition freezing (see next sections) they are shifted to the ice particle spectrum. The saturation ratio during growth and shrinking processes is iteratively calculated (Simmel and Wurzler, 2005).

Collision processes are described by the linear discrete method (Simmel et al., 2002) including the collision kernel of Kerkweg et al. (2003). By using the corresponding densities and terminal velocities, the collision kernel is appropriate for all collision processes between aerosol particles, drops, and ice particles such as growth of drops by collision/coalescence, impaction scavenging of particles by drops, contact freezing of supercooled drops, growth of ice particles by riming, and secondary ice formation., i.e. freezing of supercooled drops by collision with an ice germ.

Because of the explicit descriptions mentioned above the microphysical scheme is a useful tool to study in detail the link between aerosol particles and the evolution of cloud properties. The incorporation into an air parcel model has the advantage that all changes in the microphysical evolution of the cloud can be attributed to microphysical processes. The model improvements presented in the next sections include the following:

1. An updated particle-type dependent description of immersion freezing which is now related to the mass of insoluble particles contained in drops,
2. a modified description of contact freezing which is not only dependent on particle type but also particle size-resolved,

3. a new particle-type dependent description of deposition freezing.

All parameterizations are directly based on previous and new laboratory measurements as described in the following sections.

2.1 Immersion freezing

The previous description of immersion freezing (Diehl and Wurzler, 2004) gave the freezing rate of pure water drops containing ice nucleating particles as a function of the drop volume according to:

$$-\frac{dN_f}{dt} = N_{liq}\ B_{imm}\ V_d \exp(-a_{1,imm}\ T)\ \frac{dT}{dt} \qquad (1)$$

with N_f the number of frozen drops, N_{liq} the number of liquid drops, and the constants $a_{1,imm}$ and B_{imm}. This parameterization implicitly reflected the fact that larger drops contain more particles because of collision and coalescence of drops and impaction scavenging of aerosol particles. The previous version was replaced by a new one which is coupled directly to the mass of insoluble particles in the drops. This is possible because of the sectional distribution of drops and particles into size classes (Diehl et al., 2006).

2.1.1 Parameterizations based on laboratory data

The experimental data used as basis for the parameterizations include the following ice nucleating particle types: bacteria, pollen, feldspar, illite, and kaolinite. Murray et al. (2011) investigated kaolinite KGa-1b, Atkinson et al. (2013) K-feldspar. Illite NX was studied by Broadley et al. (2012) and recently by Hiranuma et al. (2015). The latter publication summarized the results from seventeen experimental techniques. Wex et al. (2015) include the results from seven experimental techniques using Snomax® as a proxy for bacteria. Previous data for pollen (Diehl et al., 2002; v. Blohn et al., 2005) were newly evaluated. As parameter for immersion freezing the number of active sites per unit mass n_m was selected as this is derived directly from the particle mass concentration in the drops during the experiments. Some references give as outcome from their measurements the surface density of active sites per unit particle surface n_s; however, this parameter was derived afterwards by using a specific particle surface.

For kaolinite KGa-1b, K-feldspar, tree and grass pollen, an exponential increase of n_m with temperature T was found which is described by

$$n_m = \exp\,(a_{imm} + b_{imm}\, T_s) \qquad (2)$$

with n_m in g^{-1}, a_{imm} and b_{imm} particle-related constants, $T_s = T_0 - T$, $T_0 = 0$°C, with T in °C. The constants for all particle types are listed in Table 1. Given in Table 1 are also the parameters T_{ini} and T_{lim}, representing the onset of immersion freezing during experiments and the lowest temperature which was investigated in the experiments, respectively.

Based on the best fit of the data of Murray et al. (2011) the constants in Eq. 2 were derived for kaolinite KGa-1b by using an average specific particle surface area of 11.8 $m^2\ g^{-1}$ as given by Murray et al. (2011); the result is shown in Figure 1 as orange line. The solid part of the line represents the range which is validated by measurements of Murray et al. (2011) while the dotted part shows an extrapolation towards higher temperatures. The value of T_{ini} is based on earlier measurements of Pitter and Pruppacher (1973). The same was performed for K-feldspar by using the best fit to the experimental data given by Atkinson et al. (2013) which was changed into Eq. 2 by using the specific particle surface area of 3.2 $m^2\ g^{-1}$ from Atkinson et al. (2013). The parameters are listed in Table 1, the result of Eq. 2 is shown in Figure 1 as red line. Regarding pollen, previous data from Diehl et al. (2002) and v. Blohn et al. (2005) were evaluated. From the frozen fractions of drops, the drop volume, and the mass of pollen in the drops the numbers of active sites n_m as functions of temperature were calculated according to (e.g., Murray et al., 2011):

$$n_m = -\frac{\ln\,(1 - f_{ice}(T))}{c_{pollen}\, V_{drop}} \qquad (3)$$

where $f_{ice}(T)$ is the fraction of frozen drop at temperature T, c_{pollen} the pollen concentration per drop, and V_{drop} the drop volume. Data for tree and grass pollen were summarized leading to two parameterizations for tree and grass pollen as given in Eq. 2. The constants are listed in Table 1 and the results of Eq. 2 are shown in Figure 1 as light green lines. The solid parts of the lines represent the ranges which are validated by measurements while the dotted parts show extrapolations towards lower temperatures.

Regarding illite NX and Snomax®, parameterizations were suggested by Broadley et al. (2012), Hiranuma et al. (2015), and Wex et al. (2015). To come to analogue descriptions as in the cases of the other particle types, these parameterizations were replaced by new ones following Eq. 2. Regarding illite NX, the parameterization was derived from the data reported by Hiranuma et al. (2015). The fit as given by Hiranuma et al. (2015) was changed into an ex-

pression for n_m by using the specific particle surface area of 124.4 m^2 g^{-1} of the illite NX sample (Hiranuma et al., 2015). From the non-linear curve (solid blue line in Figure 2) a linear regression line was derived which is included in Figure 1 (blue solid line). For Snomax®, it was concluded in Wex et al. (2015) that the average n_m values (given in Figure 2 as open green symbols) are very well represented by the Hartmann et al. (2012) parameterization (solid green line in Figure 2). One can notice a linear increase in the temperature range down to approximately -9°C and a further progress on a maximum value of 1.4×10^{12} g^{-1}. Thus, a linear regression curve was derived for the increase of n_m until the maximum value was reached; it is included in Figure 2 as solid green line.

It can be noted from Figure 1 that bacteria act at the highest temperatures starting not far below 0°C. Pollen lie in the range of the mineral dust particles. The differences between the mineral dust types are significant with feldspar the most efficient one, kaolinite the least efficient one.

2.1.2 Treatment of immersion freezing in the model

The previous Eq. 1 which gives the freezing rate of the supercooled drops had to be replaced by a similar expression which couples the number of active sites and the mass of insoluble particles in the drops. According to the singular description of heterogeneous freezing (Vali, 1971; Broadley et al., 2012) the frozen fraction of drops f_{ice} is given by

$$f_{ice}(T) = \frac{N_f(T)}{N_{liq}} = 1 - \exp(-n_m(T) m_{pid}) \tag{4}$$

with $N_f(T)$ the number of frozen drops at temperature T, N_{liq} the number of liquid drops, m_{pid} the mass of particles immersed in the drops, and $n_m(T)$ the number of active sites per unit mass at temperature T which is related to the cumulative nucleus spectrum $K(T)$ per unit mass per unit temperature:

$$n_m(T) = -\int_{T_0}^{T} K(T) dT \tag{5}$$

when lowering the temperature from $T_0 = 0$°C to T. From Eqs. 4 and 5 an expression for the change of the number of frozen drops ΔN_f per temperature interval ΔT can be derived (Connolly et al. (2009) :

$$\Delta N_f = N_{liq}(1 - \exp(-K(T) m_{pid} \Delta T)) \tag{6}$$

with N_{liq} the number of supercooled liquid drops and m_{pid} the mass of particles immersed in the drop. Thus, Eq. 1 can be replaced by

$$\frac{dN_f}{dt} = N_{liq} \frac{1 - \exp\left(-K(T)\, m_{pid}\, dT\right)}{dt} \tag{7}$$

As the aerosol particles are internally mixed one can assume that only a fraction of the insoluble mass per drop consists of ice nucleating material. Thus, the mass m_{pid} was reduced by a factor F_{INP} so that only this mass fraction accounts for possible numbers of active sites n_m and Eq. 7 was modified to

$$\frac{dN_f}{dt} = N_{liq} \frac{1 - \exp\left(-K(T)\, m_{pid}\, F_{INP}\, dT\right)}{dt} \tag{8}$$

A similar treatment was applied in Diehl and Wurzler (2010). From Eqs. 2 and 5 it follows:

$$K(T) = \frac{dn_m(T)}{dT} = b_{imm}\ \exp\left(a_{imm} + b_{imm}\, T_s\right) \tag{9}$$

In Eq. 9 the freezing point depression due to the content of soluble material in the drops is considered, for details see Diehl and Wurzler (2004). In the model simulations, immersion freezing starts at the particle-related temperature T_{ini}, and at temperatures below T_{lim} it is assumed that the numbers of active sites stay constant. The sizes of possibly ice nucleating particles are restricted, i.e., dust particles must be larger than 0.1 µm in diameter, bacteria are limited to their typical diameters of 0.3 to 2 µm (Matthias-Maser and Jaenicke, 1995). Pollen are large particles of 10 µm at least (Straka, 1975), however, for the present simulations a lower limit of 2 µm was selected to allow at least some freezing by pollen (see Section 3, initial dry particle number size distributions).

During the model simulations the content of insoluble particles per drop varies by several orders of magnitude which is due to the sizes of the condensation particles, the uptake of particles by the drops via impaction scavenging, and the drop collisions followed by coalescence. Thus, not all drops of the same sizes freeze at certain temperatures which describes the situation in real clouds (Diehl and Wurzler, 2004).

2.2 Contact freezing

In Diehl et al. (2006) contact freezing was described for several particle types independent of their sizes. However, measurements indicate that the size of the involved particles affects the

contact freezing efficiency in the way that efficiency increases with increasing particle size (e.g., Gorbunov et al. (2001); Hoffmann et al., 2013a; Ladino et al. 2013). Therefore, the description of Diehl et al. (2006) was modified in the way that it is now particle-size dependent.

2.2.1 Parameterizations based on laboratory data

Measurements which give a direct correlation between particle size and contact freezing efficiency are not yet available for a wider range of ice nucleating particle types. Therefore, for the present parameterization different size classes were examined. Hoffmann et al. (2013a, 2013b), and Hoffmann and Kiselev (2014, pres. comm.) performed contact freezing experiments using an electrodynamical balance with monodisperse particles of 150 to 750 nm diameter. The results showed rather low median freezing temperatures T_{50} (the temperature where 50% of an observed drop population freeze), e.g., -34°C for illite NX, -32.5°C for kaolinite Fluka and less than -25°C for Snomax®, in comparison to measurements with polydisperse particle samples.

Those experiments with polydisperse particle samples were performed at the UCLA vertical wind tunnel by Levin and Yankofsky (1983) and Pitter and Pruppacher (1973). The latter studied kaolinite and montmorillonite with particle diameters between 0.1 and 10 µm with a mode between 1 and 2 µm and measured median freezing temperatures of -12°C and -8°C, respectively. Levin and Yankofsky found a median freezing temperature of -4.5°C for bacteria. Diehl et al. (2012) investigated polydisperse mineral particles with supercooled drops suspended in an acoustic levitator. Median freezing temperatures were -11.5°C for illite NX and -8.7°C for montmorillonite K10. The latter agrees very well with the value found by Pitter and Pruppacher (1973) within the measurement error (1K). Extrapolating the data of Hoffmann et al. (2013b) for illite NX towards larger particle sizes as shown in Figure 3 indicates that a median freezing temperature of -11.5°C could be affected by dust particles with sizes between 2.3 and 3.0 µm in diameter (Diehl et al., 2012). Those particles are part of the polydisperse particle spectrum of illite NX (Hiranuma et al., 2015). Thus, one might conclude that the median freezing temperatures determined for polydisperse particle samples are affected by larger particles present in the size spectrum. This is probably the case also for previous findings measured with polydisperse particle samples.

Therefore, as an approximation, data obtained from polydisperse particle samples were used in the present parameterizations for particles with diameters mostly larger than 1 µm, at least

larger than 0.7 µm. Data obtained from monodisperse particle samples were taken for ranges around the respective particle sizes.

The experimental data used as basis for the parameterizations include the following ice nucleating particle types: bacteria, feldspar, montmorillonite, illite, and kaolinite. In most cases, a linear correlation between the frozen fraction of drops and the temperature was found. From the experimental data, regression lines were calculated which are shown in Figure 4 for various particle types (marked by different colors) and particle sizes (marked by different line styles).

Bacteria

Particle sizes of bacteria were restricted to their typical sizes with diameters between 0.3 and 2 µm (Matthias-Maser and Jaenicke, 1995). Measurements of Hoffmann and Kiselev (2014, pers. comm.) were performed with monodisperse Snomax® particles of 0.32 and 0.55 µm diameter. These data were used for size ranges from 0.3 to 0.5 µm and from 0.5 to 0.7 µm. For particles between 0.7 and 2 µm the data of Levin and Yankofsky (1983) were taken. The results are given in Figure 4 as green lines.

Mineral dust particles

For mineral dust particles, a lower size limit of 0.1 µm in diameter was assumed. Illite NX particles were investigated by Hoffmann et al. (2013b) with 0.15, 0.32, 0.55, and 0.75 µm particles. These data were taken for size ranges from 0.1 to 0.2 µm, 0.2 to 0.4 µm, 0.4 to 0.6 µm, and 0.6 to 0.8 µm. For larger particles, data from Diehl et al. (2012) were used. The results are shown in Figure 4 as blue lines. K-feldspar was investigated by Hoffmann and Kiselev (2014, pers. comm.) with 0.32 and 0.55 µm particles and by Diehl and Mitra (2014, pers. comm.) with polydisperse particles. Here three size ranges were defined, from 0.1 to 0.4 µm, 0.4 to 0.8 µm, and larger than 0.8 µm. The data are marked in Figure 4 as red lines. For kaolinite and montmorillonite, also two size ranges were specified, from 0.1 and 1 µm and larger than 1 µm. The data for the larger particles sizes were both taken from Pitter and Pruppacher (1973, polydisperse particle samples). Results from Hoffmann et al. (2013a) were used for the smaller size range of kaolinite. Under the assumption that the differences between larger and smaller INP are similar for kaolinite and montmorillonite the data for the smaller size range of montmorillonite were obtained by a parallel shifting analogue to kaolinite. In Figure 4, results for kaolinite are given in orange, results for montmorillonite in cyan.

From Figure 4 it can be noted that particles in the larger size ranges affect freezing already at temperatures around -10°C while smaller particles become active in a temperature range around -25°C. Bacteria act at the highest temperatures, kaolinite and illite at the lowest. For all particle types and sizes except bacteria smaller than 0.7 μm the frozen fraction of drops increases linearly with temperature T (given in °C) according to Diehl et al. (2006):

$$\frac{N_f}{N_{liq}} = a_{con}\, T + b_{con} \tag{10}$$

with N_f the number of frozen drops, N_{liq} the number of liquid drops colliding with inactivated particles at temperature T, and the constants a_{con} and b_{con}. Note that in Eq. 10 the frozen fraction is limited to values between 0 and 1. In Diehl et al. (2006), the constants were given for several particle types independent of their sizes while in the present parameterization the constants a_{con} and b_{con} are size-resolved. They are listed in Tables 2 and 3. In case of small bacteria the equation to calculate the frozen fraction of drops with respect to the temperature T (in °C) has the form

$$\frac{N_f}{N_{liq}} = a_{con} + b_{1,con}T + b_{2,con}T^2 + b_{3,con}T^3 \tag{11}$$

The size-resolved constants a_{con}, $b_{1,con}$, $b_{2,con}$, and $b_{3,con}$ are given in Table 2.

2.2.2 Treatment of contact freezing in the model

The description of contact freezing includes the following conditions: (1) inactivated particles have to be present, and (2) particles and supercooled drops have to collide with each other. Furthermore, the sizes of the particles allowed as activating ice nucleating particles are restricted as for deposition freezing (i.e., dust particles > 0.1 μm in diameter, bacteria 0.3 to 2 μm in diameter).

The presence of inactivated particles is always the case during the air parcel ascent because of entrainment, i.e. new inactivated particles are continuously mixed in at the edges of the simulated cloud. However, in the presently employed air parcel model the particles are in equilibrium with respect to the water vapor in their environment and, thus, they take up some water due to their size and soluble fraction. As introduced in Diehl et al. (2006) the dryness of a potential ice nucleating particle is defined by the assumption that the water mass should be smaller than half of the dry particle mass.

The second condition is considered by a collision kernel K calculated for supercooled drops and particles (Kerkweg et al., 2003; for more details see Diehl et al., 2006):

$$K = E_{coll}\left|V_{\infty,drop} - V_{\infty,ap}\right| \cdot \pi\left(r_{drop} - r_{\infty}\right)^2 \quad (12)$$

where $V_{\infty,drop}$ and $V_{\infty,ap}$ are the terminal velocities of the drop and the particle, respectively, r_{drop} and r_{ap} the drop and particle radii, respectively. The collision kernel shows highest values for collisions between large drops and particles (Diehl et al., 2006), i.e. contact freezing is most efficient when large supercooled drops and particles are present. If during the model simulations inactivated particles collide with supercooled drops the number of frozen drops is calculated. It is assumed that only a fraction F_{INP} of the aerosol particles is able to act as ice nucleating particles. Only drops which collide with those INP are allowed to freeze which is included in the following modified Eqs. 13 and 14:

$$N_f = F_{INP}\, N_{liq}\,(a_{con}\, T + b_{con}) \quad (13)$$

$$N_f = F_{INP}\, N_{liq}\,(a_{con} + b_{1,con} T + b_{2,con} T^2 + b_{3,con} T^3) \quad (14)$$

This is under the requirement that these equations are based on measurements with one drop–particle collision per freezing event so that the fraction of frozen drops in Eqs. 13 and 14 can be set equal to the freezing probability (Ladino et al., 2013). This requirement is fully achieved in the experiments of Hoffmann et al. (2013a; 2013b), and Hoffmann and Kiselev (2014, pers. comm.). During the experiments of Pitter and Pruppacher (1973), Levin and Yankofsky (1983), and Diehl et al. (2012) the number of collisions per freezing event is not documented. Single supercooled drops were freely levitated (in a wind tunnel or an acoustic levitator) while one burst of INP was blown on it. Therefore, as the particles collided almost simultaneously with the supercooled drop one could assume that in case the drop froze this was triggered by the first collision.

2.3 Deposition freezing

2.3.1 Parameterizations based on laboratory data

The experimental data used as basis include the following ice nucleating particle types: bacteria, feldspar, illite, Saharan and Asian dust. The measurements were performed with INP counters FRIDGE (**FR**ankfurt **I**mmersion and **D**eposition freezin**G** **E**xperiment) or with a continuous flow diffusion chamber (CFDC). Data for Asian and Saharan dust were taken from measurements with the NAUA FRIDGE (Ardon-Dryer and Levin, 2012, pers. comm.),

data for illite NX and Snomax® from INUIT FRIDGE experiments (Hiranuma et al., 2015; Danielczok and Bingemer, 2014, pers. comm.; Weber, 2014), and data for illite IMt1 and K-feldspar from CFDC measurements (Yakobi-Hancock et al., 2013). The Snomax® data were considered as representative for bacteria in the model simulations.

Ardon-Dryer and Levin (2012, pers. comm.) measured the activation of Saharan and Asian dust particles at different ice supersaturations and temperatures and observed an increase of the activated particles with supersaturation but no temperature dependence in the observed temperature range between -15 and -20°C. Figure 5 shows the data of Ardon-Dryer and Levin (2012) as activated fraction of particles as a function of ice supersaturation. From all data, mean values were calculated and regression lines were derived. These are included into Figure 6 as cyan and pink solid lines.

The INUIT FRIDGE measurements were performed with illite NX and Snomax® in a temperature range from -10 to -25°C. A significant temperature dependence was not observed and, therefore, the activated particle fraction was derived as a function of ice supersaturation only. As ice saturation is dependent on temperature an implicit dependence of deposition freezing on temperature is already incorporated. Regression lines were calculated based on the average values. They are given in Figure 6 as blue (illite NX) and green (Snomax®) solid lines. It can be noticed that illite NX is much more efficient than the Saharan and Asian dust particles which are characterized by a mixed composition. Asian dust mostly consists of quartz (Möhler et al., 2006) which acts in the deposition mode at lower temperatures than illite (Zimmermann et al., 2008). Also Saharan dust contains a quartz fraction of nearly one third (Möhler et al., 2006). As expected the activated fractions of Snomax® particles are the highest. Measurements with a CFDC were performed at -40°C with illite IMt1 and K-feldspar particles (Yakobi-Hancock et al., 2013). Regression lines were derived from the data and are given in Figure 6 as blue (illite IMt1) and red (K-feldspar) broken lines, respectively.

For illite NX and Snomax®, data are available not only for polydisperse particle samples but also for samples with distinct particle sizes (Danielczok and Bingemer, 2014, pers. comm.; Weber, 2014). In case of illite, monodisperse particles with diameters of 300 and 500 nm resulted in higher activated fractions for the larger particle sizes but in both cases the activated fractions were higher than in case of the polydisperse particle samples. In case of Snomax®, monodisperse particles of 100, 200, 300, and 500 nm were investigated finding again higher activated fractions for the larger particle sizes than in the polydisperse case. As particle-size

resolved measurements are not available for all particle types it was decided to treat deposition freezing size-independent in the model. As the activated fractions of the polydisperse particle samples (which are the basis of the present parameterizations) are lower than the ones of monodisperse samples, this would not lead to an overestimation of deposition freezing.

For all particle types, an exponential increase of the activated fraction with the ice supersaturation was found which is described by

$$\frac{N_{act}}{N_{total}} = \exp\left(a_{dep} + b_{dep}\, s_{ice}\right) \tag{15}$$

with N_{act} the number of activated particles, N_{total} the total particle number, s_{ice} the ice supersaturation given in %, a_{dep} and b_{dep} particle-related constants. The values of a_{dep} and b_{dep} are listed in Table 4 for the different particle types. Note that the activated fraction in Eq. 15 is limited to values between 0 and 1.

Although data were available only for ice supersaturation ranges below 25% (bacteria, illite NX, Saharan and Asian dust) and above 20% (illite IMt1 and feldspar), respectively, due to the investigated temperature ranges, it is assumed that Eq. 15 is valid for the complete ice supersaturation range. However, according to the onset of deposition freezing in the experiments, lower limits of ice supersaturation and temperature as measured during the FRIDGE experiments were set in the model. That means, deposition freezing of illite IMt1 and feldspar start at the same conditions as illite NX. In the model simulations, the two types of illite were taken as upper and lower limits and referred as illite 1 and illite 2. The values are given in Table 4.

2.3.2 Treatment of deposition freezing in the model

Conditions for deposition freezing are: (1) inactivated particles have to be present as it is required for contact freezing, i.e. the same particles may affect deposition or contact freezing. Additionally, (2) there are two size conditions. First, the inactivated particles have to exceed a critical germ size r^* in dependence of temperature and ice supersaturation which is according to Pruppacher and Klett (2010):

$$r^* = \frac{2\, M_W\, \sigma_{i,v}}{R\, T\, \rho_{ice} \ln S_{ice}} \tag{16}$$

where M_W the molecular weight of water, $\sigma_{i,v}$ the surface tension, R the universal gas constant, T the temperature, ρ_{ice} the density of ice, and S_{ice} the ice saturation ratio. However, this condition is actually redundant as it excludes particles smaller than approximately 0.01 µm and additionally size restrictions of the ice nucleating particles were assumed: dust particles larger than 0.1 µm in diameter and bacteria between their typical size range of 0.3 and 2 µm in diameter (Matthias-Maser and Jaenicke, 1995).

In each time step it is checked if temperature and ice supersaturation are above the limit values T_{ini} and $s_{ice,ini}$, if yes it is checked which available inactivated particles exceed the size limits, and from these the activated fraction is calculated. It is assumed that only a part F_{INP} of the available particles is able to act as ice nucleating particles. Therefore, the total number of particles in Eq. 15 is reduced:

$$N_{act} = F_{INP}\, N_{total} \exp\left(a_{dep} + b_{dep}\, s_{ice}\right) \qquad (17)$$

The activated particles are moved to the ice particle spectrum and grow further by water vapor deposition and they may serve as germs for secondary ice formation, i.e. they may initiate freezing of supercooled drops by collision (Diehl et al., 2006).

3 Model initiation and sensitivity studies

During the present sensitivity studies, convective clouds were simulated. In those clouds liquid drops are transferred into higher regions in the atmosphere and supercooled. Once frozen the ice particles grow further by riming (i.e. collision with other supercooled droplets) and by the deposition of water vapour (i.e. at the expense of liquid drops, the Bergeron-Findeisen process, which is typically much faster than condensation). Due to the vertical velocity large precipitation-sized ice particles can form in convective clouds and fall out as graupels, hailstones or, when they fall through the melting layer, as large raindrops. The present model simulations were initialized with a convective vertical profile where temperatures in higher altitudes were low enough to assure ice formation. It has an average lapse rate of approximately 0.6 K per 100 m without any maxima or minima (Langmann, 2004, pers. comm.), see Figure 7.

The ascent of the air parcel is driven by a temperature difference between the air bubble and its environment. Depending on the temperature difference the updraft of the air parcel proceeds at various speeds and reaches various heights with corresponding temperatures (Diehl et

al., 2006). For the present simulations, the final temperatures were -24.5°C, -29°C, and -40°C with corresponding maximum altitudes of 9 km, 9.5 km, and 11 km; the maximum vertical velocities during the ascent of the parcel were 15 m s^{-1}, 16.5 m s^{-1}, and 19 m s^{-1}.

Two different dry aerosol particle number size distributions were used to compare the effects on ice formation. One was an average continental distribution (OPAC database, Hess et al., 1998) which is a rather broad spectrum and characterized by a large number of small particles, see black line in Figure 8; its parameters are N = 7000 cm^{-3}, d = 42.4 nm, and σ = 2.24 (with N the particle number, d the diameter, and σ the standard deviation). The other one was a regional haze distribution (Reid et al. 1998) which is a rather narrow spectrum and characterized by larger particle sizes. The parameters are N = 6000 cm^{-3}, d = 0.1 μm, and σ = 1.65, see red line in Figure 8. Both rather simple mono-modal distributions were selected to avoid a mixture of effects due to ice physics and activation of aerosol particles. Thus, the effects of ice physics should be emphasized. The soluble fraction ε of the aerosol particles was set to 0.5 which is a typical value of atmospheric particles (Busch et al., 2002).

Regarding the conditions on the sizes of the ice nucleating particles as given in Section 2 (mineral dust particles larger than 0.1 μm, bacteria larger than 0.3 μm, pollen larger than 2 μm), one can conclude from Figure 8 that – in particular in the average continental case – the majority of the continental particles is too small to affect ice formation. The dry particle spectrum influences the drop spectrum which is important for immersion and contact modes. Figure 9 shows the number concentrations as a function of diameter for two different altitudes and corresponding temperatures of zero and -29°C for the two cases, average continental and regional haze particles. Because the liquid water content is the same during both model simulations, fewer but larger drops develop with the regional haze distribution and numerous but smaller drops with average continental distribution. On the other hand, as the continental spectrum is broader, collision and coalescence processes are more effective and, thus, larger drops evolve. Also given in Figure 9 are the number concentrations of the interstitial aerosol particles. Note that during the updraft inactivated aerosol particles are available for ice formation in deposition contact modes.

With these initial conditions, a multitude of sensitivity studies was performed to demonstrate the impact of ice nuclei concentrations and types on ice formation in convective mixed-phase clouds. First, single freezing processes were studied while the following parameters were varied:

- dry aerosol particle number size distribution: average continental and regional haze,
- ice nucleating particle type – biological particles and mineral dust,
- temperature difference: 3K, 2K, and 1.5 K, leading to final temperatures of -40°C, -29°C, and -24.5°C, respectively,
- fraction of potential ice nucleating particles F_{INP} – variation between 0.001 and 10%.

Afterwards, coupled freezing processes were investigated to study the competition between the different freezing processes. These were undertaken only with those parameters which resulted in higher ice formation.

4 Results and discussion

4.1 Ice water fractions and single freezing processes

To evaluate the efficiency of the different freezing processes and ice nucleating particle types, as a central diagnostic parameter the ice water fraction *IWF* was selected which is calculated from the ice water content *IWC* and the liquid water content *LWC*:

$$IWF = \frac{IWC}{LWC + IWC} \tag{19}$$

According to Korolev et al. (2003) an ice cloud is defined by $IWF > 0.9$, a liquid cloud by $IWF < 0.1$, and mixed-phase clouds by $0.1 \leq IWF \leq 0.9$. Note that in an air parcel model, the *IWF* is only influenced by in-situ ice formation processes and not by sedimentation of ice into or out of the considered parcel. In the following Tables 5 to 7, the ice water fractions as results from the sensitivity studies are listed for immersion, contact, and deposition freezing. Ice and mixed-phase clouds are marked by bold face type.

A first sight on Table 5 to 7 shows that mixed-phase or ice clouds mainly evolved from the continental particle distribution with bacteria, feldspar, or illite INP and with larger ΔT, i.e. final temperatures reaching below -25°C. The different points are discussed in detail in the following.

Particle number size distributions:

With the regional haze particles (larger particles but smaller numbers), less ice was formed in most cases than with the average continental particles (smaller particles but larger number). Less but mostly large drops develop with the regional haze distribution and many but smaller drops with average continental distribution (see Figure 9). On the other hand, a few still larg-

er drops evolved from the tail of the continental spectrum. The presence of large drops favors immersion and contact freezing (immersion mode: the drops contain more insoluble material; contact mode: the collision kernel between large drops and particles is enhanced), see Tables 5 and 6. This was suggested already by the findings of Diehl et al. (2006) and confirmed by, e.g., Lance et al. (2011) who concluded from their observations that the drop size distribution modulates ice processes in mixed-phase clouds.

In the deposition mode (Table 7), no drops but only the interstitial particles are relevant. More inactivated particles are present in the regional haze case than in the continental case (see Figure 9) so that because of the higher competition between the many particles, less ice particles develop by the deposition of water vapor.

Freezing modes:

Immersion freezing affects the most mixed-phase clouds with ice water fractions of more than 0.5 and even ice clouds with all kinds of investigated INP (Table 5). Pollen are, of course, disadvantaged because of their large sizes, kaolinite particles are the less efficient mineral dust particles while bacteria and feldspar are the most efficient INP. With bacteria, freezing occurred already with potential fractions of INP F_{INP} as low as 0.001%. With mineral dust, potential fractions of INP F_{INP} of 0.01% (feldspar, illite) or 0.1% (kaolinite) were necessary. Ice formation was sensitive to the type of mineral dust as well as to the potential fraction of INP. For instance, under the same conditions an ice cloud could form with feldspar but a mixed-phase cloud with only a small ice water fraction with kaolinite.

In the contact mode, there is very little ice formation (Table 6). Only liquid clouds formed with the regional haze particle distribution but in case of the average continental distribution at least some mixed-phase clouds formed with ice water fractions between 0.1 and 0.3. High potential fractions of INP F_{INP} of 10% were required. Bacteria did not affect ice formation, this probably results from the restricted particle sizes. The type of mineral dust decides whether mixed-phase clouds are formed (feldspar, montmorillonite) or not (illite, kaolinite).

Effective deposition INP are bacteria, feldspar, and illite while the mixed particle samples Saharan and Asian dust form liquid clouds only. Mixed-phase clouds formed with high potential INP fractions F_{INP} between 1 and 10%. The results for the different mineral dust types are rather similar but mixed-phase clouds were formed with pure minerals only but not with mixtures (Saharan and Asian dust) which are dominated by quartz (see Section 2.3.1).

Ervens et al. (2011) who investigated the impact of immersion and deposition freezing modes on ice formation in mixed-phase clouds stated that immersion freezing formed less ice than deposition freezing because of lower onset temperatures in the immersion mode. However, this could not be confirmed in the present study. Newer laboratory measurements which were used as basis of the parameterizations showed in contrary higher initial temperatures in the immersion mode than in the deposition mode (see Tables 1 and 4 with references therein) and, thus, immersion freezing produced more ice than deposition freezing. This agrees, on the other hand, with the findings of de Boer et al. (2011) and Lance et al. (2011) that liquid-dependent ice nucleation modes are dominant.

Temperature difference ΔT and final temperature

In all freezing modes, cases with the lowest temperature difference (ΔT = 1.5K) and the corresponding highest final temperature of -24.5°C showed hardly ice formation. Exceptions are only cases with bacteria and feldspar in the immersion mode (Table 5). Contact ice formation did not occur with lower ΔT as the temperatures reached during the ascent of the air parcel were not low enough to give the more effective smaller particles the chance to act (Table 6). In the deposition mode, obviously temperatures below -25°C are required to develop mixed-phase clouds (Table 7) as at higher temperatures the ice supersaturation is still too low. On the other hand, the largest ΔT of 3K also hindered ice formation in contact and deposition modes which might be affected by the presence of less interstitial particles.

4.2 Comparison to measured INP numbers

In this section a discussion is included how realistic the assumed concentrations of INP are which lead to partial or complete cloud glaciation.

Immersion freezing

Regarding the cases of immersion freezing listed in Table 5, one has to look at the composition of cloud residuals which was investigated in several field campaigns. E.g., Kamphus et al. (2010) measured 8% minerals in cloud droplet residuals; Hiranuma et al. (2013) found 3% mineral dust particles in cloud droplet residuals for all particle sizes and particle-size resolved measurements indicated enhanced fractions for larger particles up to 17%. In the model simulations mixed-phase clouds were formed already with potential INP fractions between 0.01 and 1%. Thus, the dominant role of immersion freezing with mineral dust seems to be validated. It is confirmed by the fact that during INUIT field campaigns (Worringen et al., 2014;

Schmidt et al., 2015) fractions of mineral dust up to 40% in ice residuals were observed. Similar numbers between 30 and 40% are reported by Kamphus et al. (2010) in ice particle residuals.

Bacteria need to be present as potential INP only as low as 0.001 to 0.01% to affect mixed-phase clouds, pollen with 1% potential INP. For pollen these numbers do probably not represent realistic cases; however, the pollen cases were anyway rather artificial as such large particles (> 10 μm) were actually not part of the aerosol particle spectrum. Bacteria concentrations in cloud water are given as average values of, e.g., 1.5×10^9 m^{-3} (Sattler et al., 2001), 2×10^{10} m^{-3} (Bauer et al. 2002), and 7×10^4 m^{-3} (Amato et al., 2005; see also the review paper of Delort et al., 2010). Unfortunately, field measurements which give the number fractions of bacteria or primary biological aerosol particles (PBAP) related to the total concentrations of in-droplet particles are not available so far. An estimation was undertaken based on the results of Bauer et al. (2002). From field measurements in a continental background site they determined the numbers of bacterial and fungi cells in cloud water and calculated the corresponding amount which would contribute to the amount of organic carbon (OC). For bacteria this contribution was estimated as 0.01%. Analyses of cloud droplet residuals show, e.g., fractions of 3% (Twohy and Anderson, 2008) and 9% (Hiranuma et al., 2013) organic carbon. Based on these numbers one could assume that 0.0003 to 0.0009% of the material contained in cloud drops consists of bacteria. This comes near the fraction of potential ice nucleating particles F_{INP} of 0.001% which affects mixed-phase clouds via immersion freezing (see Table 5). Joly et al. (2014) investigated the ice nucleation efficiency of cloud water samples and distinguished total and biological INP. They estimated that − assuming that all biological INP were bacteria − in the temperature range between -8 and -12°C 0.6 to 3.1% of the bacterial cells present in the cloud water samples could have acted as INP. Taking into account these values, a fraction F_{INP} of 0.001% is probably still an overestimation of realistic bacterial ice nucleating particles in cloud drops.

Thus, one may conclude that the atmospheric immersion freezing with mineral dust particles will play a dominant role while ice formation via immersion freezing of bacteria might take place in some extreme cases only.

Contact and deposition freezing

According to the cases listed in Tables 6 and 7, the formation of mixed-phase clouds via contact or deposition freezing requires that 10% of the background aerosol consists of potential

ice nucleating particles. Measurements during an INUIT field campaign on the high alpine site Jungfraujoch (Schmidt et al., 2015) indicate a fraction of 1% minerals of the background aerosol; however, this value might be enhanced for continental situations in lower altitudes. A closer look was taken on the total number concentrations of ice nucleating particles acting as contact and deposition freezing particles during the model simulations. As shown in Figure 9 for two different altitudes and corresponding temperatures, interstitial aerosol particles were always present during the ascent of the air parcel. Among these, only particles larger than 0.1 µm in diameter were allowed to act as ice nucleating particles. The total number concentrations of those during the model simulations reach values up to 4×10^5 m^{-3} for the average continental and up to 2×10^6 m^{-3} for the regional haze distribution. Thus, fractions of potential ice nucleating particles F_{INP} of 10% resulted in particle concentrations available for deposition and contact nucleation of at the most 4×10^4 m^{-3} and 2×10^5 m^{-3}, respectively.

In Saharan dust events, Bangert et al. (2012) measured particle number concentrations up to 5×10^7 m^{-3}. In Hande et al. (2014), simulated mineral dust number concentrations are 4×10^5 m^{-3} on average up to extreme values of 5.8×10^6 m^{-3}. Thus, the numbers of potential INP used in the model simulations do not exceed realistic particle concentrations of mineral dust.

Near-surface concentrations of bacteria range between 1×10^3 m^{-3} and 5×10^5 m^{-3} depending on ecotypes (Burrows et al., 2009) but these values are certainly not reached in upper cloud regions. On the other hand, DeLeon-Rodriguez et al. (2013) reported from field measurements in low- and high-altitude air masses that bacterial cells represented nearly 20% of the total particles in the diameter range between 0.25 and 1 µm. This is approximately the size range of potential ice nucleating particles in the present model simulations. For even larger particles in the coarse mode high fractions of PBAP (primary biological particles) are also reported by Manninen et al. (2014). However, the numbers of potential INP used in the model simulations probably overestimate real bacteria concentrations.

Considering these factors one may conclude that the conditions for atmospheric deposition and contact freezing could be sufficient in some cases to form mixed-phase clouds from primary ice formation by mineral dust particles. In some extreme cases, the formation of mixed-phase clouds might be possible via deposition nucleation on bacteria. On the other hand, the initial particle spectra used for the present model simulations contain little amounts of particles larger than 1 µm (see Figure 8) which would be able to act as contact ice nucleating par-

ticles much more efficiently (see Section 2.2.1). Thus, in cases where larger INP are present in or around atmospheric clouds contact freezing might be significantly enhanced.

4.3 Ice particle spectra, single and coupled freezing processes

In this section only simulations with the most efficient ice formation are treated, i.e. using the average continental particle distribution and a medium $\Delta T = 2K$ leading to final temperatures of -29°C. The potential fractions F_{INP} were set to 10% for feldspar, illite, montmorillonite, and kaolinite. Bacteria and pollen were not considered here as those high values of F_{INP} are not realistic (see discussion in Section 4.2). Figure 10 shows the ice particle number size distributions at different altitudes and corresponding temperatures for single deposition, contact, and immersion freezing processes which are discussed in the next paragraphs.

The ice particle spectra affected by immersion freezing are rather narrow starting with a particle diameter of 1 µm due to the smallest drop size. However, larger drops around 30 µm in diameter were frozen first as their content of insoluble particles is higher. With decreasing temperature, also smaller drops can freeze while ice particles grow by the deposition of water vapour and by riming, i.e. the ice particle spectra broaden in both directions. Finally, they are still smaller than the ones formed by deposition freezing. The differences between the dust types are much more evident than in the other modes and the final ice particle numbers are higher, in particular for feldspar.

In the contact mode, the simulated ice particle spectrum is even somewhat narrower. At temperatures around -20°C, the maximum of the drop number concentration lies at 30 µm. This indicates that large supercooled drops froze by collisions with larger particles as in this temperature range smaller particles are hardly efficient as contact INP. Lowering the temperature down to -29°C extends the ice particle spectra towards larger sizes, i.e. the ice particles grow by the deposition of water vapor and by riming but still only little amounts of small drops are freezing. Thus, contact freezing is strongly controlled by the collision kernel. The number concentrations of ice particles formed on feldspar and montmorillonite are rather similar at -30°C but strongly different at -21°C. This is due to the fact that smaller feldspar particles are active at higher temperatures as smaller montmorillonite particles (see Figure 4).

The ice particle spectra due to deposition freezing start with small sizes and develop towards larger sizes during the ascent of the cloud. This indicates that firstly, as primary ice formation, small ice particles are formed due to the sizes of the involved particles (0.1 µm at least up to 3

μm maximum, see the initial particle spectra in Figure 8). Afterwards, these pristine ice particles serve as nuclei for secondary ice formation, i.e. by collisions with supercooled liquid drops. This process produces ice particles of larger sizes, see maximum around 40 μm in Figure 10. Furthermore, all ice particles grow by the deposition of water vapor and by riming leading to ice particles larger than 100 μm. Thus, a broad spectrum of ice particles evolved from deposition freezing. The number concentrations vary by one order of magnitude from illite2 to feldspar. The oscillations of the spectra on the left hand side are an artefact effect of the size classes of the particles acting as INP starting with 0.1 μm diameter; they vanish if the lower size of the INP is limited by the critical radius only (Eq. 16).

Coupled cases were simulated to investigate the competition between contact and immersion modes as both freeze supercooled drops, and the competition between contact and deposition freezing as both interact with inactivated particles. The following combinations were studied: 1) feldspar and 2) illite1 as for these particle types parameterizations for all freezing modes are available based on INUIT measurements. Additionally, some mixed cases were investigated, i.e. one INP type for one freezing mode, another INP type for the other freezing mode. These were for coupled contact and immersion freezing 3) montmorillonite + kaolinite, 4) feldspar + kaolinite. These cases were selected to combine weaker immersion freezing INP (kaolinite) with stronger contact freezing INP (feldspar and montmorillonite), see Figure 12a. For coupled deposition and contact freezing the mixed cases were 3) illite2 + montmorillonite, 4) Saharan dust + feldspar. As can be noted from Tables 5 to 7, the ice water fractions evolved from feldspar INP are similar for deposition and contact freezing but significantly higher for immersion freezing. The effects from illite1 INP differ between the freezing modes (immersion highest, contact lowest). The combination illite2 + montmorillonite in deposition and contact modes was selected because the resulted ice water fractions were similar which is also the case for the combination montmorillonite + kaolinite in contact and immersion modes.

In contrast, the fourth combinations Saharan dust + feldspar (deposition and contact) and feldspar + kaolinite (contact and immersion) were chosen as the ice water fractions evolved by contact freezing were higher. Figure 11 shows the ice particle number size distributions at different altitudes and corresponding temperatures for coupled deposition and contact and coupled contact and immersion freezing processes.

One can note from Figure 11 that deposition and contact freezing are hardly in competition. The narrow ice particle spectrum due to contact freezing alone is enhanced towards smaller sizes due to deposition freezing. Small ice particles are formed by deposition freezing due to the sizes of the involved particles (0.1 to 3 μm), large ice particles are formed by contact freezing due to the sizes of involved liquid drops (30 to 50 μm, see Figure 10). When first ice formation is observed via contact and deposition freezing at temperatures around -20°C, in the contact mode only dust particles larger than 0.4 μm (feldspar), 0.8 μm (illite), and 1 μm (kaolinite) are active (see Figure 4), thus, all smaller particles and fractions of the larger particles are available for deposition freezing. Even at lower temperatures, still small particles remain for deposition freezing as these are less efficient to collide with drops. The common ice particle spectra of coupled deposition and contact freezing are as broad as the ones from single deposition freezing but the number concentrations in the larger size range are enhanced in cases with efficient contact freezing, i.e. with feldspar and montmorillonite INP.

Regarding coupled contact and immersion freezing, here the latter is the dominant process. Using the same particle types there is no effect visible from contact freezing (feldspar, illite1). However, in cases where the contact INP are more efficient than the immersion INP (feldspar or montmorillonite in contrast to kaolinite) the number concentrations are slightly enhanced in the size range larger than 90 μm (see Figure 10 and 11).

The total numbers of liquid drops and ice particles in cm^{-3} as a function of temperature are given in Figure 12. Results from single freezing processes are shown in Figure 12a. In the upper part of the figure, liquid drop numbers are shown as solid lines. The black line represent liquid drop numbers on the order of 8×10^2 cm^{-3} which applies for all cases except immersion freezing with feldspar. Below, in all remaining plot lines ice particle numbers are given in Figure 12a for the three single freezing processes as colored lines (the colors describe the types of INP) with different line styles: solid lines for immersion freezing (feldspar, illite1, and kaolinite), dotted lines for contact freezing (feldspar, montmorillonite, and illite), and broken lines for deposition freezing (feldspar, illite1, illite2, and Saharan dust).

From the ice particle numbers at the lowest temperature of -29°C, one can clearly distinguish between cloud types: ice particle numbers around 1 cm^{-3} represent an ice cloud (immersion freezing with feldspar), ice particle numbers around 1×10^{-8} cm^{-3} represent a liquid cloud (i.e. the ice water fraction is smaller than 0.1; contact freezing with illite), and ice particle numbers between 1×10^{-4} cm^{-3} and 1×10^{-2} cm^{-3} represent mixed-phase clouds (all other cases). In the

only case of ice cloud formation (immersion with feldspar) the liquid drop number is affected as well: it is reduced to 5×10^{1} cm^{-3} (i.e. the ice water fraction is larger than 0.9), see red solid line in the upper part of the figure.

It can be seen that the development of ice particle numbers with decreasing temperature via immersion freezing (colored solid lines) is similar to the development of the numbers of active sites immersed in the drops with decreasing temperature (shown in Figure 1). In contrast, contact freezing (dotted lines) is not ruled by the temperature alone but also by the collision efficiencies between potential INP and supercooled drops (see Section 2.2) while deposition freezing (broken lines) is ruled by the ice supersaturation (see Section 2.3) which, of course, increases with decreasing temperature.

Comparing the liquid drop numbers to the ice particle numbers one notes that the differences are approximately between 4 and 6 orders of magnitude in cases of mixed-phase clouds and still more than one order of magnitude in case of the ice cloud. This indicates that the glaciation of the clouds proceeds mainly by the growth of ice particles at the expense of liquid drops (Bergeron-Findeisen process or riming). Here, some effects are presumably overestimated as from the air parcel no cloud particle sedimentation is possible.

Figure 12b shows results for the coupled freezing processes. Again liquid drop numbers are given as solid lines in the upper part of the figure. The black line represents liquid drop numbers which applies for all cases except immersion + contact freezing with feldspar. Lower plot lines in Figure 12b show ice particle numbers for the two coupled freezing processes as colored lines (the colors describe the types of INP) with different line styles: solid lines for immersion + contact freezing (feldspar, illite1, kaolinite + feldspar, kaolinite + montmorillonite), and broken lines for deposition + contact freezing (feldspar, illite1, illite2 + montmorillonite, Saharan dust + feldspar).

Ice clouds and mixed-phase clouds differ in the ice particle numbers at the lowest temperature of -29°C: ice particle numbers around 1 cm^{-3} represent an ice cloud (immersion + contact freezing with feldspar), and ice particle numbers between 5×10^{-4} cm^{-3} and 1×10^{-2} cm^{-3} represent mixed-phase clouds (all other cases). In the only case of ice cloud formation the liquid drop number is affected as well, see red solid line in the upper part of the figure.

It is obvious that in those cases where one process is inferior the ice particle numbers are completely determined by the dominant process. This is the case in coupled immersion and contact freezing with feldspar and illite1 but not with kaolinite + feldspar and kaolinite +

montmorillonite where the effects of contact freezing are visible at lower temperatures (< -20°C). Coupled deposition and contact freezing shows the same results as for deposition freezing alone in case of illite. In the other cases, feldspar, illite2 + montmorillonite, and Saharan dust + feldspar, there are at least some small enhancements visible at temperatures lower than -20°C when contact freezing becomes more efficient.

4.4 Comparison of presently simulated ice particle numbers to previous literature data

In this section results from the model simulations are compared to data from previous model simulations and atmospheric measurements. As comparison parameter the number of ice particles formed at the end of the air parcel ascent was used as shown in Figure 12. These simulations were performed with the continental particle distribution, dT=2K, and F_{INP}=10%. I.e. for F_{INP} values lower than 10% less ice particle numbers are formed.

Eidhammer et al. (2009) used an air parcel model to perform intercomparisons of three heterogeneous ice nucleation parameterizations which linked aerosol types and numbers to ice particle number concentrations. One of these was the previous immersion freezing parameterization of Diehl and Wurzler (2004) that has been replaced by a new one in this study. This description was related to the volume of liquid similar as the well-known Bigg parameterization (Bigg, 1953). The criticisms was that some constraints are required that limit the number of potential ice nucleating particles. The present parameterization is related to the insoluble particle mass contained in the drops and the constraint is given by the factor F_{INP} in Eq. 8. Ice particle numbers found by Eidhammer et al. (2009) with the Diehl and Wurzler (2004) description were in the range of 5×10^{-2} to 5×10^{-1} cm^{-3} while results from the current simulations are on the order of 1×10^{-3} cm^{-3} for mixed-phase clouds (see Figure 12, immersion freezing).

In Ervens and Feingold (2012) the effects of five ice nucleation schemes for immersion freezing with particles showing surface characteristics like kaolinite particles on the properties of mixed-phase clouds were compared in air parcel studies. The present parameterization of immersion freezing is similar to the so-called deterministic scheme of Ervens and Feingold (2012) which includes a cumulative activation spectrum as a function of temperature. Using this scheme in their parcel model with polydisperse INP, they found ice particle numbers from 2×10^{-4} to 1×10^{-3} cm^{-3}. In spite of differences between the present and previous air

parcel studies (e.g., height of parcel elevation) the present results of immersion freezing with kaolinite particles, i.e. 3.5×10^{-4} cm^{-3} (see Figure 12a) agree very well.

Fan et al. (2010) simulated two deep convective clouds from field campaigns, one cloud formed under clean conditions, the other under polluted conditions with biomass burning. They used a three-dimensional cloud-resolving model with different immersion/condensation/deposition and homogeneous ice nucleation parameterizations. The averaged cloud properties for their clean case showed ice particle numbers between 1.3×10^{-2} and 1.5×10^{-2} cm^{-3} in dependence of the ice nucleation schemes. For the comparison coupled immersion and deposition freezing was simulated with kaolinite acting in the immersion mode, Saharan dust in the deposition mode (not shown in Figure 12b). These two particle types might represent the behaviour of "mean" atmospheric INP. During the calculations dT was varied by 2K, 2.5K, and 3K. The final ice particle numbers were 4.8×10^{-4} cm^{-3}, 2.2×10^{-2} cm^{-3}, and 6.4×10^{-1} cm^{-3}, respectively, and, thus, best agreement with a deep convective cloud was obtained with dT=2.5K.

Kulkarni et al. (2012) used Arizona test dust (ATD) and kaolinite to experimentally investigate and model deposition freezing. However, their measured activated fractions of particles as a function of ice supersaturation were at least one to two orders of magnitude larger than the ones used as basis for the parameterizations in the present study. Therefore, not surprisingly, the modeled ice particle numbers found by Kulkarni et al. (2012) were between 2×10^{-3} and 1×10^{-2} cm^{-3} and up to two orders of magnitude larger than the ones found in the present simulations (1.4×10^{-4} cm^{-3} for Saharan dust, 7.2×10^{-4} cm^{-3} for illite2, 1.8×10^{-3} cm^{-3} for illite1, and 4.5×10^{-3} cm^{-3} for feldspar, see Figure 12a).

Observations of atmospheric clouds reported ice particle number concentrations of 1×10^{-4} to 10 cm^{-3} in convective clouds (Hobbs et al., 1980), 1×10^{-5} to 5×10^{-2} cm^{-3} in mixed phase clouds (McFarquhar et al.; 2007; modeled by Fridlind et al., 2007); 1×10^{-1} to 1 cm^{-3} in ice clouds (Krämer et al., 2009). Thus, the ice particle numbers formed during the present model simulations, i.e. 1×10^{-4} to 1×10^{-2} cm^{-3} for mixed-phase clouds and 9×10^{-1} cm^{-3} for ice clouds (see Figure 12) represent the status of real atmospheric clouds.

5 Summary and conclusions

In this paper improvements and modifications of the spectral-bin microphysics embedded in an adiabatic air parcel model with entrainment as described in Diehl et al. (2006) are present-

ed. They include (1) a particle-type dependent parameterization of immersion freezing, (2) a particle-type and size-resolved parameterization of contact freezing, and (3) a particle-type dependent description of deposition freezing. Sensitivity studies with the modified version of the microphysics package demonstrated the impact of ice nuclei concentrations and types on ice formation in convective mixed-phase clouds. Single and coupled freezing processes were studied and the following parameters were varied: initial aerosol particle number size distributions, final temperature, types of INP, and the fractions of potential INP.

The majority of mixed-phase and ice clouds were formed at temperatures below -25°C, with the average continental particle number size distribution and with immersion freezing, even with smaller values of F_{INP} (fractions of potential INP).

First, larger drops freeze in the immersion mode because they contain more particulate material. During the updraft of the cloud and corresponding lower temperatures, the ice particle spectra develop towards smaller sizes. Contact freezing is limited by the collision kernel between supercooled drops and potential ice nucleating particles. Large particles collide more often with large drops. Because they are more efficient contact INP than smaller particles this leads at first to the formation of larger ice particles. Smaller particles which represent in general the majority of the particle spectrum become effective at lower temperatures and, thus, contact freezing becomes relevant below -25°C. During coupled immersion and contact freezing immersion freezing is the dominant process in cases with the same INP types (feldspar, illite). In mixed cases where contact INP are more efficient than immersion INP (feldspar or montmorillonite with kaolinite), contact freezing contributes similarly as immersion freezing to ice formation. In such cases sufficient liquid drops are available for contact freezing.

The importance of deposition freezing lies in secondary ice formation: at first, small pristine ice particles are formed due to the sizes of the involved particles which trigger the freezing of supercooled drops by collisions. Thus, a broader ice particle spectrum is generated than by immersion and contact freezing. Regarding coupled contact and deposition freezing, there is hardly competition because both start moderately at higher temperatures so that inactivated particles are present for both freezing modes.

The most effective ice nucleating particles are bacteria, feldspar, and illite; of minor importance are pollen, montmorillonite, and kaolinite. Ice formation by immersion freezing is very sensitive to the different mineral dust types leading to ice particle numbers varying by three orders of magnitude.

From the model results it can be concluded that the formation of mixed-phase and ice clouds in convective situations is promoted by (1) the immersion freezing mode, (2) broad drop size spectra containing small as well as large drops, (3) insoluble particles composed by bacteria, feldspar, and illite, and (4) temperatures below -25°C.

The dominance of the immersion mode confirms the findings of de Boer et al. (2011) and Lance et al. (2011) about the importance of liquid-dependent ice nucleation modes. The role of contact freezing remained still unclear. In Diehl et al. (2006) it was estimated to be the most efficient process; however, this was because of assuming high freezing efficiencies for all particle sizes. Thus, the effects in the present model simulations with the modified contact freezing description should be closer to the real situation in the atmosphere. Contact freezing might be enhanced in atmospheric situations where particles larger than 1 µm are present in higher amounts. The dependence of ice formation on the properties of the liquid drop size spectrum was also observed by Lance et al. (2011). This should be investigated in more detail but was not the main focus of the present simulations which concentrated more on the impact of ice nucleating particle types.

Bacteria as primary biological particles were found to affect mixed-phase or even ice clouds; however, the critical factor is the availability in atmospheric environment and clouds. Together with estimations of their atmospheric occurrence the present model simulations indicate that they are probably not involved in significant ice formation. This has been suggested already by Phillips et al. 2009, Diehl and Wurzler (2010), and Paukert and Hoose (2014). Thus, mineral dust particles seem to be the most important INP. The model results indicate that ice formation by immersion freezing is similarly sensitive to the mineral dust types as to the potential fractions of INP. Therefore, the composition of dust particles decides their impact on ice nucleation in clouds; essential components are feldspar and illite. In particular, the investigation of typical atmospheric mixtures of mineral dust is relevant.

The microphysical package presented here was included into an air parcel model which has the advantage that all changes in the microphysical evolution of the cloud can be attributed to microphysical processes. On the other hand, some compromises are required concerning the cloud dynamics including some well-known weaknesses as precipitation sized cloud particles do not sediment but stay inside the parcel. As they are not removed from the parcel they could grow to unrealistic sizes. This can happen notably in the ice phase and lead to an overestimation of cloud glaciation. Some more limitations which should be considered are related to

immersion and contact freezing. During the cloud model runs each drop contains insoluble material serving as immersion ice nucleus because the particles in the model are internally mixed. In a real cloud there might be drops which do not contain any potential ice nucleating material. Furthermore, the values of F_{INP} used in the model represent maximum estimations as not all dust particles are able to affect freezing at atmospheric temperatures. For contact freezing, the amount of interstitial inactivated particles is limited in an air parcel model while in a real cloud there might be more inactivated particles at the edges or beneath the cloud.

The further goal is to implement the new microphysical scheme into to a more complex state-of-the-art model system. For this purpose presently the 3D cloud model COSMO-SPECS (Grützun et al, 2008) is employed. This model contains the microphysical scheme as used in Diehl et al. (2006) within the adiabatic parcel model which is replaced by the microphysical scheme presented here. Such an improvement will allow more complex model simulations including the formation of precipitation which will enlighten the role of ice nucleating particles in atmospheric clouds.

Acknowledgements

This work is part of the research group INUIT (Ice Nuclei research UnIT) FOR1525 and was supported by the Deutsche Forschungsgemeinschaft under grant DI 1539/1-1. We appreciate the INUIT laboratory and field groups for providing their experimental data as basis of parametrizations and for helpful discussions. Thanks to Karin Ardon-Dryer for providing unpublished material. We would like to thank Corinna Hoose for fruitful discussions and helpful comments and suggestions.

References

Amato, P., Ménager, M., Sancelme, M., Laj, P., Mailhot, G., and Delort, A.-M.: Microbial population in cloud water at the Puy de Dôme: implications for the chemistry of clouds. Atmos. Environ. 39, 4143-4153, 2005.

Ansmann, A., Althausen, D., Müller, D., Seifert, P., Freudenthaler, V., Heese, B., Wiegner, M., Pisani, G., Knippertz, P., and Dubovik, O.: Influence of Saharan dust on cloud glaciation in southern Morocco during Saharan mineral dust experiment. J. Geophys. Res., 113, doi:10.1029/2007JD008 785, 2008.

Atkinson, J.D., Murray, B.J., Woodhouse, M.T., Whale, T.F., Baustian, K.J., Carslaw, K.S., Dobbie, S., O'Sullivan, D., and Malkin, T.L.: The importance of feldspar for ice nucleation by mineral dust in mixed-phase clouds. Nature, 498, 355-358, doi:10.1038/nature12278, 2013.

Bangert, M., Nenes, A., Vogel, B., Vogel, H., Barahona, D., Krydis, V.A., Kumar, P., Cottmeier, C., and Blahak, U.: Saharan dust event impacts on cloud formation and radiation over Western Europe. Atmos. Chem., Phys., 12, 4045-4063, doi:10.51/ACP-12-4045-2012, 2012.

Bauer, H., Kasper-Giebl, A., Löflund, M., Giebl, H., Hitzenberger, R., Zibuschka, F., and Puxbaum, H.: The contribution of bacteria and fungal spores to the organics content of cloud water, precipitation and aerosols. Atm. Res., 64, 109-119, 2002.

Bigg, E.K.: The formation of atmospheric ice crystals by the freezing of droplets. Quart. J. Roy. Meteor. Soc., 79, 510-519, 1953.

Broadley, S.L., Murray, B.J., Herbert, R.J., Atkinson, J.D., Dobbie, S., Malkin, T.L., Condliffe, E., and Neve, L.: Immersion mode heterogeneous ice nucleation by an illite rich powder representative of atmospheric mineral dust. Atmos. Chem. Phys., 12, 287-307, doi:10.5194/acp-12-287-2012, 2012.

Burrows, S.M., Elbert, W., Lawrence, M.G., and Pöschl, U.: Bacteria in the global atmosphere – Part 1: Review and synthesis of literature data for different ecosystems. Atmos. Chem. Phys., 9, 9263-9280, 2009.

Busch, B., Kandler, K., Schütz, L., and Neusüß, C.: Hygroscopic properties and water soluble volume fraction of atmospheric particles in the diameter range from 50 nm to 3.8 µm during LACE 98, J. Geophys. Res., 107 D, LAC 2-1 – LAC 2-11, 2002.

Connolly, P.J., Möhler, O., Field, P.R., Saathoff, H., Burgess, R. Choularton, T., and Gallagher, M.: Studies of heterogeneous freezing by three different desert dust samples. Atmos. Chem. Phys., 9, 2805-2825, doi:10.5194/acp-9-2805-2009, 2009.

de Boer, G., Morrison, H., Shupe, M. D., and Hildner, R.: Evidence of liquid dependent ice nucleation in high-latitude stratiform clouds from surface remote sensors. Geophys. Res. Lett., 38, L01803, doi:10.1029/2010GL046016, 2011.

DeLeon-Rodriguez, N., Lathem, T.L., Rodriguez-R, L.M., Barazesh, J.M., Anderson, B.E., Beyersdorf, A.J., Ziemba, L.D., Bergin, M., Nenes, A., and Konstantinidis, K.T.: Microbiome

of the upper troposphere: Species composition and prevalence, effects of tropical storms, and atmospheric implications. P. Natl. Acad. Sci., 110, 2575–2580, doi:10.1073/pnas.1212089110, 2013.

Delort, A.-M., Vaïtilingom, M., Amato, P., Sancelme, M., Parazols, M., Mailhot, G., Laj, P., and Deguillaume, L: A short overview of the microbial population in clouds: Potential roles in atmospheric chemistry and nucleation processes. Atmos. Res., 98, 249-260.

DeMott, P., Prenni, A.J., McMeeking, G.R., Sullivan, R.C., Petters, M.D., Tobo, Y., Niemand, M., Möhler, O., Snider, J.R., Wang, Z., and Kreidenweis, S.M.: Integrating laboratory and field data to quantify the immersion freezing ice nucleation activity of mineral dust particles. Atmos. Chem. Phys., 15, 393-409, doi:10.15194/acp-15-393-2015, 2015.

Diehl, K., and Wurzler, S.: Heterogeneous drop freezing in the immersion mode: Model calculations considering soluble and insoluble particles in the drops. J. Atmos. Sci., 61, 2063-2072, 2004.

Diehl, K., and Wurzler, S.: Air parcel model simulations of a convective cloud: Bacteria acting as immersion ice nuclei. Atmos. Environ., 44, 4622-4628, 2010.

Diehl, K., Matthias-Maser, S., Mitra, S.K., and Jaenicke, R.: The ice nucleating ability of pollen. Part II: Laboratory studies in immersion and contact freezing modes. Atmos. Res., 61, 125-133, 2002.

Diehl, K., Simmel, M., and Wurzler, S.: Numerical simulations of the impact of aerosol properties and drop freezing modes on the glaciation, microphysics, and dynamics of clouds, J. Geophys. Res., 111, D07202, doi:10.1029/2005JD005884, 2006.

Diehl, K., M. Simmel, and Wurzler, S.: Effects of drop freezing on microphysics of an ascending cloud parcel under biomass burning conditions. Atmos. Environ., 41, 303-314, 2007.

Diehl, K., Schmithüsen, H., Debertshäuser, M., Borrmann, S., and Mitra, S.K.: Laboratory investigations of contact and immersion freezing of mineral dust using an acoustic levitator, Proceedings European Aerosol Conference, Granada, Spain, 2012.

Duft, D., and Leisner, T: Laboratory evidence for volume-dominated nucleation of ice in supercooled water microdroplets, Atmos. Chem. Phys., 4, 1997-2000, 2004.

Eidhammer, T., DeMott, P.J., and Kreidenweis, S.M.: A comparison of heterogeneous ice nucleation parameterizations using a parcel model framework. J. Geophys. Res., 114, D06202, doi:10.1029/2008JD011095, 2009.

Ekman, A.M.L., Engström, A., and Wang, C.: The effect of aerosol composition and concentration on the development and anvil properties of a continental deep convective cloud. Q. J. R. Met. Soc., 133, 1439-1452, 2007.

Ervens, B., and Feingold, G.: On the representation of immersion and condensation freezing in cloud models using different nucleation schemes. Atmos. Chem. Phys., 12, 5807-5826, doi:10.5194/acp-12-5807-2012, 2012.

Ervens, B., and Feingold, G.: Sensitivities of immersion freezing: Reconciling classical nucleation theory and deterministic expressions. J. Geophys. Res. Lett., 40, 3320-3324, doi:10.1002/grl.50580, 2013.

Ervens, B., Feingold, G., Sulia, K., and Harrington, J.: The impact of microphysical parameters, ice nucleation mode, and habit growth on the ice/liquid partitioning in mixed-phase Arctic clouds. J. Geophys. Res., 116, D17205, doi:10.10029/2011JD015729, 2011.

Fan, J., Comstock, J.M., Ovchinnikov, M., McFarlane, S.A., McFarquhar, G., and Allen, G.: Tropical anvil characteristics and water vapour of the tropical tropopause layer: Impact of heterogeneous and homogeneous freezing parameterizations. J. Geopys. Res., 115, doi:10.1029/2009JD012696, 2010.

Fridlind, A.M., Ackerman, A.S., McFarquhar, G., Zhang, G., Poellot, M.R., DeMott, P.J., Prenni, A.J., and Heymsfield, A.J.: Ice properties of single-layer stratocumulus during the Mixed-Phase Arctic Cloud Experiment: 2. Model results. J. Geophys. Res., 112, D24202, doi:10.1029/2007JD008646, 2007.

Gilmore, M.S., Straka, J. M., and Rasmussen, E.N.: Precipitation and Evolution Sensitivity in Simulated Deep Convective Storms: Comparisons between liquid-only and simple ice and liquid phase microphysics. Mon. Wea. Rev., 132, 1897-1916, 2004.

Gorbunov, B., Baklanov, A., Kakutkina, N., Windsor, H.L., and Toumi, R.: Ice nucleation on soot particles. J. Aerosol Sci., 32, 199-215, 2001.

Grützun, V., Knoth, O., and Simmel, M: Simulation of the influence of aerosol particle characteristics on clouds and precipitation with LM-SPECS: Model description and first results. Atmos. Res., 90, 233-242, 2008.

Hande, L.B., Engler, C., Hoose, C., and Tegen, I.: Seasonal variability of Saharan desert dust and ice nucleating particles over Europe. Atm. Chem. Phys. Discuss., 14, 32071-32092, doi:10.5194/acpd-14-32071-2014, 2014.

Hess, M., Koepke, P., and Schult, I.: Optical properties of aerosols and clouds: The software package OPAC. Bull. Am. Met. Soc., 79, 831-844, 1998.

Hiranuma, N., Brooks, S.D., Moffet, R.C., Glen, A., Laskin, A., Gilles, M.K., Liu, P., Macdonald, A.M., Strapp, J.W., and McFarquar, G.M.: Chemical characterization of individual particles and residuals of cloud droplets and ice crystals collected on board research aircraft in the ISDAC 2008 study. J. Geophys. Res., 118, 6564-6579, doi:10.1002/jgrd.50484, 2013.

Hiranuma, N., Augustin-Bauditz, S., Bingemer, H. , Budke, C., Curtius, J., Danielczok, A., Diehl, K., Dreischmeier, K., Ebert, M., Frank, F., Hoffmann, N., Kandler, K., Kiselev, A., Koop, T., Leisner, T., Möhler, O., Nillius, B., Peckhaus, A. , Rose, D., Weinbruch, S., Wex, H., Boose, Y., DeMott, P. J. , Hader, J. D., Hill, T. C. J., Kanji, Z. A., Kulkarni, G., Levin, E. J. T., McCluskey, C. S., Murakami, M., Murray, B. J., Niedermeier, D., Petters, M. D., O'Sullivan, D., Saito, A., Schill, G. P. , Tajiri, T., Tolbert, M. A., Welti, A., Whale, T. F., Wright, T. P., and Yamashita, K.: A comprehensive laboratory study on the immersion freezing behavior of illite NX particles: a comparison of seventeen ice nucleation measurement techniques. Atmos. Chem. Phys., 15, 2489-2518, doi:10.5194/acp-15-2489-2015, 2015.

Hobbs, P.V., Politovich, M.K., and Radke, L.F.: The structure of summer convective clouds in Eastern Montana. I. Natural clouds. J. Appl. Met., 19, 645-663, 1980.

Hoffer, T.E.: A laboratory investigation of droplet freezing. J. Meteor., 18, 766-778, 1961.

Hoffmann, N., Kiselev, A., Rzesanke, D., Duft, D., and Leisner, T.: Experimental quantification of contact freezing in an electrodynamic balance. Atmos. Meas. Tech., 6, 2373-2382, doi:10.5194/amt-6-2373-2013, 2013a.

Hoffmann, N., Duft, D., Kiselev, A., and Leisner, T.: Contact freezing efficiency of mineral dust aerosols studied in an electrodynamic balance: Quantitative size and temperature dependence for illite particles. Faraday Discuss., 165, 383-390, doi:10.1039/C3FD00033H, 2013b.

Hoose, C., Lohmann, U., Erdin, R., and Tegen, I.: The global influence of dust mineralogical composition on heterogeneous ice nucleation in mixed-phase clouds, Environ. Res. Lett., 3, 025003-025017, 2008.

INUIT Research group website: www.ice-nuclei.de.

Joly, M., Amato, P., Deguillaume, L., Monier, M., Hoose, C., and Delort, A.-M.: Quantification of ice nuclei active at near 0°C temperatures in low-altitude clouds at the Puy de Dôme atmospheric station. Atmos. Chem., Phys., 14, 8185-8195, doi:10.5194/acp-14-8185-2014, 2014.

Kamphus, M., Ettner-Mahl, M., Klimach, T., Drewnick, F., Keller, L., Cziczo, D.J., Mertes, S., Borrmann, S., and Curtius, J.: Chemical composition of ambient aerosol, ice residues and cloud droplet residues in mixed-phase clouds: single particle analysis during the Cloud and Aerosol Characterization Experiment CLACE6. Atm. Chem. Phys., 10, 80777-8095, doi:10.5194/acp-10-8077-2010. 2010.

Kerkweg, A., Wurzler, S., Reisin, T., and Bott, A.: On the cloud processing of aerosol particles: An entraining air parcel model with two-dimensional spectral cloud microphysics and a new formulation of the collection kernel, Quart. J. Roy. Meteor. Soc., 129, 1-18, 2003.

Khain, A., Ovtchinnikov, M., Pinsky, M., Pokrovsky, A., and Krugliak, H.: Notes on the state-of-the-art numerical modeling of cloud microphysics. Atmos. Res., 55, 159-224, 2000.

Koop, T., Bertram, A.K., Molina, L.T., and Molina, M.J.: Phase transitions in aqueous NH_4HSO_4 solutions. J. Phys. Chem., 103, 9042-9048, 1999.

Koop, T., Beiping, L., Tsias, A., and Peter, T.: Water activity as the determinant for homogeneous ice nucleation in aqueous solutions. Nature, 406, 611-614, 2000.

Korolev, A.V., Isaac, G.A., Cober, S.G., Strapp, J.W., and Hallett, J.: Microphysical characterization of mixed-phase clouds. Q. J. R. Meteorol. Soc., 129, 39-65, 2003.

Krämer, M., Schiller, C., Afchine, A., Bauer, R., Gensch, I., Mangold, A., Schlicht, S., Spelten, S., Sitnikov, N., Borrmann, S., de Reus, M., and Spichtinger, P.: Ice supersaturations and cirrus cloud crystal numbers. Atmos. Chem. Phys., 9, 3505-3522, 2009.

Kulkarni, G., Fan, J., Comstock, J.M., Liu, X., and Ovchinnikov, M.: Laboratory measurements and model sensitivity studies of dust deposition ice nucleation. Atmos. Chem., Phys., 12, 7295-7308, doi:10.5194/acp-12-7295-2012, 2012.

Ladino Moreno, L.A., Stetzer, O., and Lohmann, U.: Contact freezing: a review of experimental studies. Atmos. Chem. Phys., 13, 9745-9769, doi:10.5194/acp-13-9745-2013, 2013.

Lance, S., Shupe, M.D., Feingold, G., Brock, C.A., Cozic, J., Holloway, J.S., Moore, R.H., Nenes, A., Schwarz, J.P., Spackman, J.R., Froyd, K.D., Murphy, D.M., Brioude, J., Cooper, O.R., Stohl, A., and Burkhart, J.F.: Cloud condensation nuclei as a modulator of ice processes in Arctic mixed-phase clouds. Atmos. Chem., Phys., 11, 8003-8015, doi:10.5194/acp-11-8003-2011, 2011.

Lee, S.S., Donner, L.J., and Phillips, V.T.J.: Impacts of aerosol chemical composition on microphysics and precipitation in deep convection. Atmos. Res., 94, 220-237, 2009.

Leroy, D., Monier, M., Wobrock, W., and Flossmann, A.I.: A numerical study of the effects of the aerosol particle spectrum on the development of the ice phase and precipitation formation. Atmos. Res., 80, 15-45; doi:10.1016/j.atmosres.2005.06.007, 2006.

Levin, Z., and Yankofsky, S.A.: Contact versus immersion freezing of freely suspended droplets by bacterial ice nuclei, J. Clim. Appl. Met., 22, 1964-1966, 1983.

Lohmann, U., and Diehl, K.: Sensitivity studies of the importance of dust nuclei for the indirect aerosol effect on stratiform mixed-phase clouds. J. Atmos. Sci., 63, 968-982, 2006.

Manninen, H.E., Bäck, J., Sihto-Nissilä, S.-L., Huffman, J.A., Pessi, A.-M., Hiltunen, V., Aalto, P.P., Hidalgo, P.J., Hari, P., Saarto, A., Kulmala, M., and Petäjä, T.: Patterns in airborne pollen and other primary biological aerosol particles (PBAP), and their contribution to aerosol mass and number in a boreal forest. Boreal Env. Res., 19 (suppl. B), 383–405, 2014.

Matthias-Maser, S., and Jaenicke, R.: Size distribution of primary biological aerosol particles with radii ≥ 0.2 µm. J. Atmos. Res.. 39, 279-286, 1995.

McFarquhar, G., Zhang, G., Poellot, M.R., Kok, G.L., MaCoy, R., Tooman, T., Fridlind, A., and Heymsfield, A.J.: Ice properties of single-layer stratocumulus during the Mixed-Phase Arctic Cloud Experiment: 2. Observations. J. Geophys. Res., 112, D24201, doi:10.1029/2007JD008633, 2007.

Möhler, O., Field, P.R., Connolly, P., Benz, S., Saathoff, H., Schnaiter, M., Wagner, R., Cotton, R., Krämer, M., Mangold, A., and Heymsfield, A. J.: Efficiency of the deposition mode ice nucleation on mineral dust particles. Atmos. Chem. Phys., 6, 3007-3021, 2006.

Murray, B.J., Wilson, T.W., Broadly, S.L., and Wills, R.H.: Heterogeneous freezing of water droplets containing kaolinite and montmorillonite particles, Atmos. Chem. Phys., 11, 4191-4207, doi:10.5194/acp-11-4191-2011, 2011.

Niemand, M., Möhler, O., Vogel, B., Vogel, H., Hoose, C., Connolly, P., Klein, H., Bingemer, H., DeMott, P., Skrotzki, J., and Leisner, T.: A particle-surface-area-based parameterization of immersion freezing on desert dust particles. J. Atmos. Sci., 69, 3077-3092, 2012.

Paukert, M., and Hoose, C.: Modeling immersion freezing with aerosol-dependent prognostic ice nuclei in Arctic mixed-phase clouds. J. Geophys. Res. Atmos., 119, 9073-9092, doi:10.1002/2014JD021917, 2014.

Phillips, V.T.J., Donner, L.J., and Garner, S.T.: Nucleation processes in deep convection simulated by a cloud-system-resolving model with double-moment bulk microphysics, J. Atmos. Sci., 64, 738-761, 2007.

Phillips, V.T.J., DeMott, P.J., and Andronache, C.: An empirical parameterization of heterogeneous ice nucleation for multiple chemical species of aerosol. J. atmos. Sci., 65, 2757-2783, 2008.

Phillips, V.T.J., Andronache, C., Christner, B., Morris, C.E., Sands, D.C., Bansemer, A., Lauer, A., McNaughton, C., and Seman, C.: Potential impacts from biological aerosols on ensembles of continental clouds. Biogeosci., 6, 987-1014, 2009.

Pitter, R.L., and Pruppacher, H.R.: A wind tunnel investigation of freezing of small water drops falling at terminal velocity in air, Quart. J. Roy. Meteor. Soc., 99, 540-550, 1973.

Pratt, K.A., DeMott, P.J., French, J.R., Wang, Z., Westphal, D.L., Heymsfield, A.J., Twohy, C.H., Prenni, A.J., and Prather, K.A.: In situ detection of biological particles in cloud ice-crystals. Nature Geoscience, 2, 398-401, doi:10.1038/ngeo521, 2009.

Pruppacher, H.R., Klett, J.D.: Microphysics of Clouds and Precipitation. 2nd rev. exp. ed., Atmospheric and Oceanographic Sciences Library, 18, Springer Science & Business Media, 2010.

Reid, J.S., Hobbs, P.V., Ferek, R.J., Blake, D.R., Martins, J.V., Dunlap, M.R., and Liousse, C.: Physical, chemical, and optical properties of regional hazes dominated by smoke in Brazil. J. Geophys. Res., 103, 32059-32080, 1998.

Sattler, B., Puxbaum, H., and Psenner, R.: Bacterial growth in supercooled cloud droplets. Geophys. Res. Lett., 28, 239-242, 2001.

Schmidt, S., Schneider, J., Klimach, T., Mertes, S., Schenk, L.P., Curtius, J., Kupiszewski, P., Hammer, E., Vochezer, P., Lloyd, G., Ebert, M., Kandler, K., Weinbruch, S., and Borrmann, S.: In-situ single submicron particle composition analysis o fice residuals from mountain-top mixed-phase clouds in Central Europe. Atmos. Chem. Phys. Discuss., 15, 4677-4724, doi:10.5194/acpd-15-4677-2015, 2015.

Simmel, M., and Wurzler, S.: Condensation and nucleation in sectional cloud microphysical models based on the linear discrete method. Atm. Res., 80, 218-236, 2006.

Simmel, M., Trautmann, T., and Tetzlaff, G.: Numerical solution of the stochastic collection equation - Comparison of the linear discrete method with other methods, Atmos. Res., 61, 135-148, 2002.

Simmel, M., Diehl, K., and Wurzler, S.: Numerical simulation of the microphysics of an orographic cloud: Comparison with measurements and sensitivity studies. Atmos. Environ., 39, 4365-4373, 2005.

Storelvmo, T., Kristjánsson, J. E., and Lohmann, U.: Aerosol influence on mixed-phase clouds in CAM-Oslo, J. Atmos. Sci., 65, 3214–3230, 2008.

Straka, H.: Pollen- und Sporenkunde. Fischer Verlag, Stuttgart, 1975.

Twohy, C.H., and Anderson, J.R.: Droplet nuclei in non-precipitating clouds: composition and size matter. Environ. Res. Letters., 3, 045002, doi:10.1088/1748-9326/4/045002, 2008.

van den Heever, S.C., Carrió, G.G., Cotton, W.R., DeMott, P.J., and Prenni, A.J.: Impacts of Nucleating Aerosol on Florida Storms. Part I: Mesoscale Simulations. J. Atmos. Sci., 63, 1752-1775, 2006.

v. Blohn, N., Mitra, S.K., Diehl, K., and Borrmann, S.: The ice nucleating ability of pollen. Part III: New laboratory studies in immersion and contact freezing modes including more pollen types. Atm. Res., 78, 182-189, 2005.

Weber, D,: Eisnukleation von Aerosolen: Laborexperimente und Messung von Schiffsemissionen. M.Sc.-thesis, Goethe University, Frankfurt/M., 2014.

Wex, H., Augustin-Bauditz, S., Boose, Y., Budke, C., Curtius, J., Diehl, K., Dreyer, A., Frank, F., Hartmann, S., Jantsch, E., Kanji, Z.A., Kiselev, A., Koop, T., Möhler, O., Nieder-

meier, D., Nilius, B., Rösch, M., Rose, D., Schmidt, C., Steinke, I. , and Stratmann, F.: Intercomparing different devices for the investigation of ice nucleating particles using Snomax as test substance. Atmos. Chem. Phys., 15, 1463-1485, doi:10.5194/acp-15-1463-2015, 2015.

Worringen, A., Kandler K., Benker, N., Dirsch, T., Weinbruch, S., Mertes, S., Schenk, L., Kästner, U., Frank, F., Nillius, B., Bundke, U., Rose, D., Curtius, J., Kupiszewski, P., Weingartner, E., Schneider, J., Schmidt, S., and Ebert, M.: Single-particle characterization of ice-nucleating particles and ice particle residuals sampled by three different techniques. Atmos. Chem. Phys. Discuss., 14, 23027–23073, doi:10.5194/acpd-14-23027-2014, 2014.

Yakobi-Hancock. J.D., Ladino, L.A., and Abbatt, J.P.D.: Feldspar minerals as efficient deposition ice nuclei. Atmos. Chem. Phys., 13, 11175-11185, doi:10.5194/acp-13-11175-2013, 2013.

Zimmermann, F., Weinbruch, S., Schütz, L., Hofmann, H., Ebert, M., Kandler, K., and Worringen, A.: Ice nucleating properties of the most abundant mineral dust phases. J. Geophys. Res., 113, D23204, doi:10.1029/2008JD010655, 2008.

particle type	a_{imm}	b_{imm}	T_{ini} °C	T_{lim} °C
bacteria (1)	6.41344	2.33592	-2	-9.139
tree pollen (2;3)	7.16249	0.62053	-9	-38
grass pollen (2;3)	9.9731	0.030301	-12	-38
feldspar (4)	2.10379	1.038	-5	-25
illite (5)	-1.77473	0.89507	-10	-37
kaolinite (6)	-4.61608	0.8881	-13	-37

Table 1: Values of immersion freezing constants in Eq. 2. Based on data from (1) Wex et al., 2015; (2) Diehl et al., 2002; (3) v. Blohn et al., 2005; (4) Atkinson et al., 2013; (5) Hiranuma et al., 2015; (6) Murray et al., 2011.

particle type and size	a_{con}	$b_{1,con}$	$b_{2,con}$	$b_{3,con}$
bacteria				
(1) 0.3 µm ≤ d_{ap} < 0.5 µm	-1.36581	-0.26367	-0.01511	-2.84911
(1) 0.5 µm ≤ d_{ap} < 0.7 µm	-0.55381	-0.10712	-0.00616	-1.16822
	a_{con}	b_{con}		
(2) 0.7 µm ≤ d_{ap} < 2 µm	-0.264	-0.742		

Table 2: Values of contact freezing constants in Eqs. 10 and 11. Based on data from (1) Hoffmann and Kiselev, 2014, pers. comm., who used Snomax® as a proxy for bacteria and (2) Levin and Yankofsky, 1983. The latter values were used in Diehl et al., 2006.

particle type and size	a_{con}	b_{con}
illite		
(1) 0.1 µm < d_{ap} ≤ 0.2 µm	-0.0306	-0.9980
(1) 0.2 µm < d_{ap} ≤ 0.4 µm	-0.0359	-1.0838
(1) 0.4 µm < d_{ap} ≤ 0.6 µm	-0.0812	-2.2989
(1) 0.6 µm < d_{ap} ≤ 0.8 µm	-0.1210	-3.3452
(2) 0.8 µm < d_{ap}	-0.1863	-1.6076
montmorillonite		
(3) 0.1 µm < d_{ap} ≤ 1 µm	-0.1014	-2.3899
(4) 1 µm < d_{ap}	-0.1014	-0.3277
kaolinite		
(5) 0.1 < d_{ap} ≤ 1 µm	-0.1285	-3.6792
(6) 1 µm < d_{ap}	-0.1007	-0.6935
feldspar		
(7) 0.1 < d_{ap} ≤ 0.4 µm	-0.1033	-2.0585
(7) 0.4 < d_{ap} < 0.8 µm	-0.1484	-2.7154
(8) 0.8 µm < d_{ap}	-0.34964	-0.13095

Table 3: Values of contact freezing constants in Eq. 10. Based on data from (1) Hoffmann et al., 2013b; (2) Diehl, 2012; (3) Extrapolation; (4) and (6) Pitter and Pruppacher, 1973, used in Diehl et al., 2006; (5) Hoffmann et al. (2013a); (7) Hoffmann and Kiselev, 2014, pers. comm.; (8) Diehl and Mitra (2014, pers. comm.).

particle type	a_{dep}	b_{dep}	T_{ini} °C	$s_{ice,ini}$ %
bacteria (1)	-12.65977	0.33382	-10 (1)	3 (1)
feldspar (2)	-14.58404	0.23576	-13 (1)	6 (1)
illite 1 (1)	-12.79648	0.15451	-13 (1)	6 (1)
illite 2 (2)	-15.11871	0.19669	-13 (1)	6 (1)
Saharan dust (3)	-13.39669	0.10058	-18 (3)	11 (3)
Asian dust (3)	-14.98495	0.09756	-15 (3)	8 (3)

Table 4: Values of deposition freezing constants a_{dep} and b_{dep} in Eq. 15 and values of lower limits of temperature T_{ini} and ice supersaturation $s_{ice,ini}$. Based on data from (1) Danielczok and Bingemer, 2014, pers. comm.; (2) Yakobi-Hancock et al., 2013; (3) Ardon-Dryer and Levin, 2012, pers. comm.

immersion freezing										
AP	regional haze					average continental				
F_{INP} (%)	**0.001**	**0.01**	**0.1**	**1**	**10**	**0.001**	**0.01**	**0.1**	**1**	**10**
dT = 3K T_{fin} = -40°C										
bacteria	**0.27**	**0.94**	**0.99**	**1.0**	**1.0**	0.03	**0.27**	**0.91**	**0.99**	**1.0**
pollen	< 0.01	< 0.01	< 0.01	< 0.01	< 0.01	< 0.01	0.02	0.08	**0.15**	**0.17**
feldspar	< 0.01	**0.12**	**0.74**	**1.0**	**1.0**	< 0.01	**0.10**	**0.37**	**0.93**	**1.0**
illite	< 0.01	0.01	**0.14**	**1.0**	**1.0**	< 0.01	**0.19**	**0.43**	**0.70**	**1.0**
kaolinite	< 0.01	< 0.01	< 0.01	**0.64**	**0.81**	< 0.01	< 0.01	**0.12**	**0.34**	**0.60**
dT = 2K T_{fin} = -29°C										
bacteria	**0.26**	**0.86**	**0.99**	**1.0**	**1.0**	**0.13**	**0.43**	**0.86**	**0.99**	**1.0**
pollen	< 0.01	< 0.01	< 0.01	< 0.01	< 0.01	< 0.01	< 0.01	0.02	**0.13**	**0.33**
feldspar	< 0.01	0.02	**0.21**	**0.71**	**1.0**	0.08	**0.34**	**0.56**	**0.80**	**0.93**
illite	< 0.01	< 0.01	< 0.01	< 0.01	0.02	< 0.01	< 0.01	0.04	**0.24**	**0.47**
kaolinite	< 0.01	< 0.01	< 0.01	< 0.01	< 0.01	< 0.01	< 0.01	< 0.01	0.02	**0.15**
dT = 1.5K T_{fin} = -24.5°C										
bacteria	**0.11**	**0.61**	**0.96**	**1.0**	**1.0**	0.05	**0.25**	**0.69**	**0.97**	**1.0**
pollen	< 0.01	< 0.01	< 0.01	< 0.01	< 0.01	< 0.01	< 0.01	< 0.01	< 0.01	0.03
feldspar	< 0.01	< 0.01	< 0.01	0.03	**0.24**	< 0.01	< 0.01	0.03	**0.35**	**0.59**
illite	< 0.01	< 0.01	< 0.01	< 0.01	< 0.01	< 0.01	< 0.01	< 0.01	< 0.01	0.01
kaolinite	< 0.01	< 0.01	< 0.01	< 0.01	< 0.01	< 0.01	< 0.01	< 0.01	< 0.01	< 0.01

Table 5: Ice water fractions from sensitivity studies with immersion freezing. Liquid clouds: $IWF < 0.1$, **mixed-phase clouds: $0.1 \leq IWF \leq 0.9$, ice clouds: $IWF > 0.9$**.

contact freezing						
AP	regional haze			average continental		
F_{INP} (%)	0.1	1	10	0.1	1	**10**
dT = 3K **T_{fin} = -40°C**						
bacteria	< 0.01	< 0.01	< 0.01	< 0.01	< 0.01	< 0.01
feldspar	< 0.01	< 0.01	< 0.01	< 0.01	< 0.01	0.06
montmorillonite	< 0.01	< 0.01	< 0.01	< 0.01	< 0.01	0.04
illite	< 0.01	< 0.01	< 0.01	< 0.01	< 0.01	< 0.01
kaolinite	< 0.01	< 0.01	< 0.01	< 0.01	< 0.01	< 0.01
dT = 2K **T_{fin} = -29°C**						
bacteria	< 0.01	< 0.01	< 0.01	< 0.01	< 0.01	< 0.01
feldspar	< 0.01	< 0.01	< 0.01	< 0.01	< 0.01	**0.23**
montmorillonite	< 0.01	< 0.01	< 0.01	< 0.01	< 0.01	**0.12**
illite	< 0.01	< 0.01	< 0.01	< 0.01	< 0.01	< 0.01
kaolinite	< 0.01	< 0.01	< 0.01	< 0.01	< 0.01	< 0.01
dT = 1.5K **T_{fin} = -24.5°C**						
bacteria	< 0.01	< 0.01	< 0.01	< 0.01	< 0.01	< 0.01
feldspar	< 0.01	< 0.01	< 0.01	< 0.01	< 0.01	0.01
montmorillonite	< 0.01	< 0.01	< 0.01	< 0.01	< 0.01	< 0.01
illite	< 0.01	< 0.01	< 0.01	< 0.01	< 0.01	< 0.01
kaolinite	< 0.01	< 0.01	< 0.01	< 0.01	< 0.01	< 0.01

Table 6: Ice water fractions from sensitivity studies with contact freezing. Liquid clouds: *IWF* < 0.1, **mixed-phase clouds: 0.1 ≤ *IWF* ≤ 0.9, ice clouds: *IWF* > 0.9**.

deposition freezing								
AP	regional haze				average continental			
F_{INP} (%)	0.01	0.1	1	**10**	0.01	0.1	**1**	**10**
dT = 3K T_{fin} = -40°C								
bacteria	< 0.01	< 0.01	0.05	**0.52**	< 0.01	0.02	**0.14**	**0.42**
feldspar	< 0.01	< 0.01	< 0.01	< 0.01	< 0.01	0.02	**0.10**	**0.31**
illite 1	< 0.01	< 0.01	< 0.01	< 0.01	< 0.01	< 0.01	0.02	**0.13**
illite 2	< 0.01	< 0.01	< 0.01	< 0.01	< 0.01	< 0.01	0.01	**0.10**
Saharan dust	< 0.01	< 0.01	< 0.01	< 0.01	< 0.01	< 0.01	< 0.01	0.01
Asian dust	< 0.01	< 0.01	< 0.01	< 0.01	< 0.01	< 0.01	< 0.01	< 0.01
dT = 2K T_{fin} = -29°C								
bacteria	< 0.01	< 0.01	< 0.01	0.06	< 0.01	0.04	**0.27**	**0.51**
feldspar	< 0.01	< 0.01	< 0.01	< 0.01	< 0.01	< 0.01	0.07	**0.34**
illite 1	< 0.01	< 0.01	< 0.01	< 0.01	< 0.01	< 0.01	0.03	**0.22**
illite 2	< 0.01	< 0.01	< 0.01	< 0.01	< 0.01	< 0.01	0.01	**0.11**
Saharan dust	< 0.01	< 0.01	< 0.01	< 0.01	< 0.01	< 0.01	< 0.01	0.02
Asian dust	< 0.01	< 0.01	< 0.01	< 0.01	< 0.01	< 0.01	< 0.01	< 0.01
dT = 1.5K T_{fin} = -24.5°C								
bacteria	< 0.01	< 0.01	< 0.01	< 0.01	< 0.01	< 0.01	< 0.01	< 0.01
feldspar	< 0.01	< 0.01	< 0.01	< 0.01	< 0.01	< 0.01	< 0.01	< 0.01
illite 1	< 0.01	< 0.01	< 0.01	< 0.01	< 0.01	< 0.01	< 0.01	< 0.01
illite 2	< 0.01	< 0.01	< 0.01	< 0.01	< 0.01	< 0.01	< 0.01	< 0.01
Saharan dust	< 0.01	< 0.01	< 0.01	< 0.01	< 0.01	< 0.01	< 0.01	< 0.01
Asian dust	< 0.01	< 0.01	< 0.01	< 0.01	< 0.01	< 0.01	< 0.01	< 0.01

Table 7: Ice water fractions from sensitivity studies with deposition freezing. Liquid clouds: $IWF < 0.1$, **mixed-phase clouds: $0.1 \leq IWF \leq 0.9$, ice clouds: $IWF > 0.9$**.

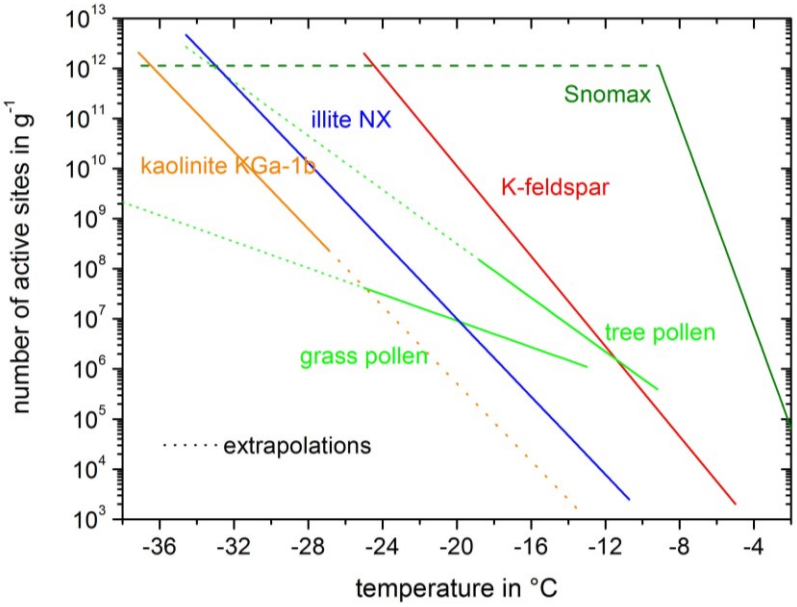

Figure 1: Numbers of active sites per unit mass as a function of temperature calculated by Eq. 2 with constants given in Table 1 for various particle types in the immersion mode. Based on laboratory data of immersion freezing experiments (Diehl et al., 2002, v. Blohn et al., 2005, pollen; Murray et al., 2011, kaolinite KGa-1b; Atkinson et al., 2013, K-feldspar; Hiranuma et al., 2015, illite NX; Wex et al., 2015, Snomax®).

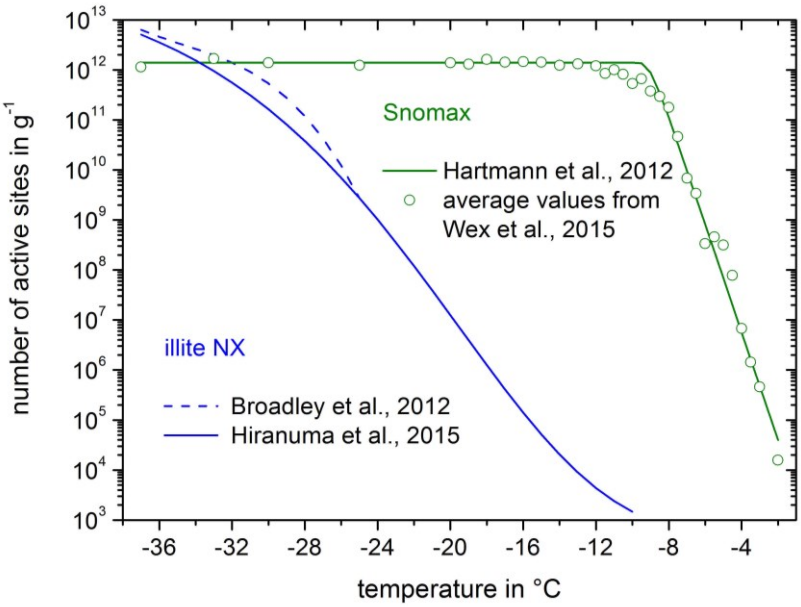

Figure 2: Numbers of active sites per unit mass as a function of temperature. Parameterizations for illite NX and Snomax® based on the outcome of laboratory immersion freezing experiments.

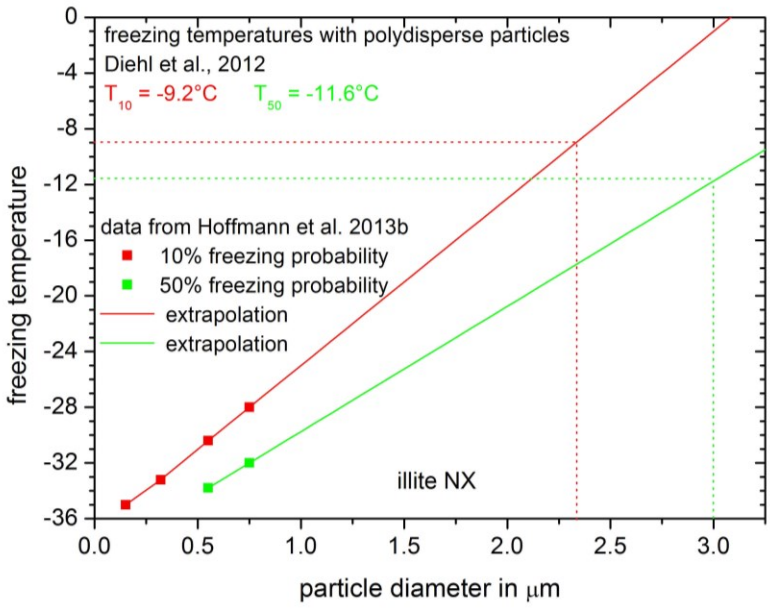

Figure 3: Freezing temperatures as a function of particle diameter for illite NX in the contact mode. Extrapolations to larger particle sizes.

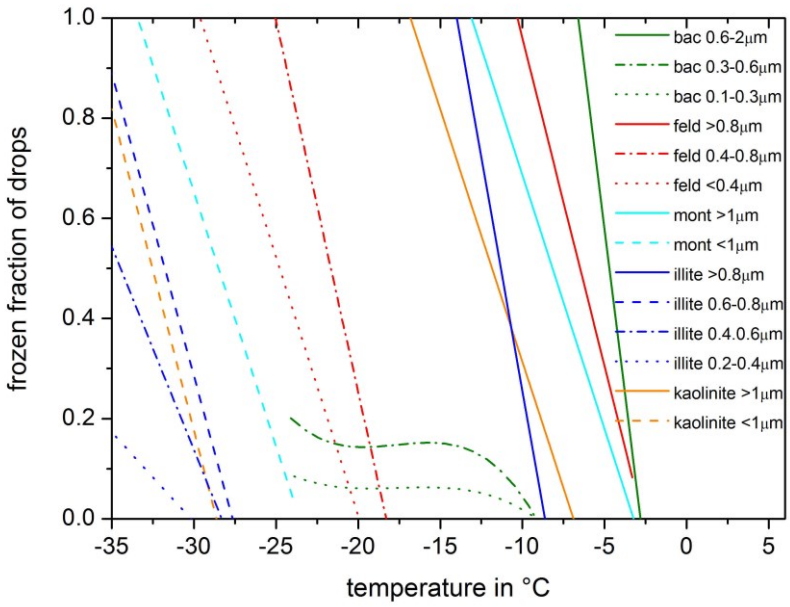

Figure 4: Frozen fraction of drops by contact freezing as a function of temperature for various particle types and sizes, marked by different colors and line styles. Calculated by Eqs. 10 and 11, respectively, with constants given in Tables 2 and 3 for various particle types, based on the outcome of laboratory experiments (Pitter and Pruppacher, 1973; Levin and Yankofsky, 1983; Diehl, 2012; Hoffmann et al., 2013a,b; Hoffmann and Kiselev, 2014, pers. comm.; Diehl and Mitra, 2014, pers. comm.).

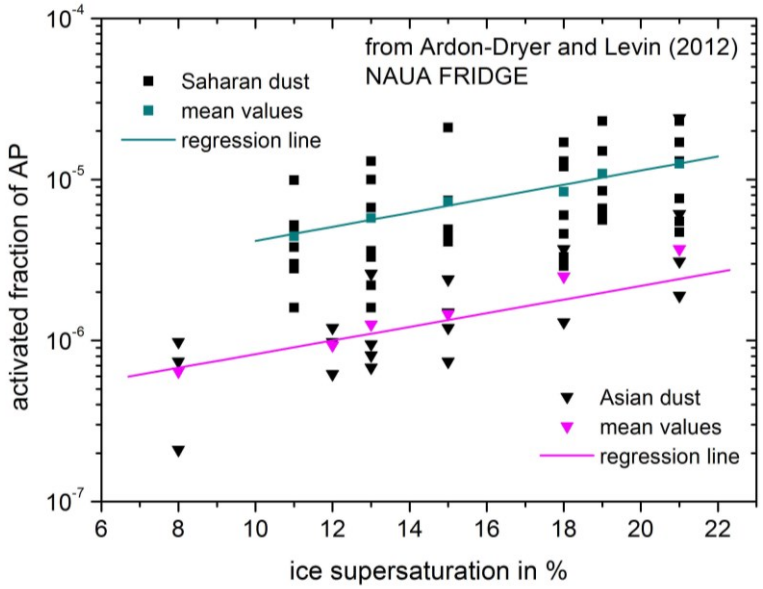

Figure 5: Activated fraction of particles in the deposition freezing mode as a function of ice supersaturation for Saharan and Asian dust. Data from Ardon-Dryer and Levin (2012, pers. comm.).

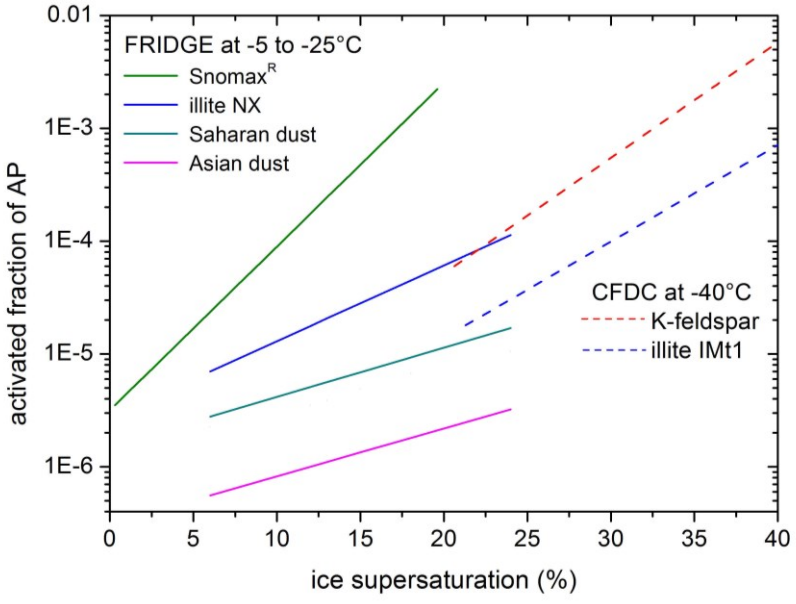

Figure 6: Activated fraction of particles in the deposition freezing mode as a function of ice supersaturation for various particle types. Regression lines based on data from Ardon-Dryer and Levin (2012, pers. comm.; Saharan and Asian dust), Yakobi-Hancock et al. (2013; K-

feldspar and illite IMt1), Danielczok and Bingemer (2014, pers. comm., Snomax® and illite NX). Described by Eq. 15 with constants in Table 4.

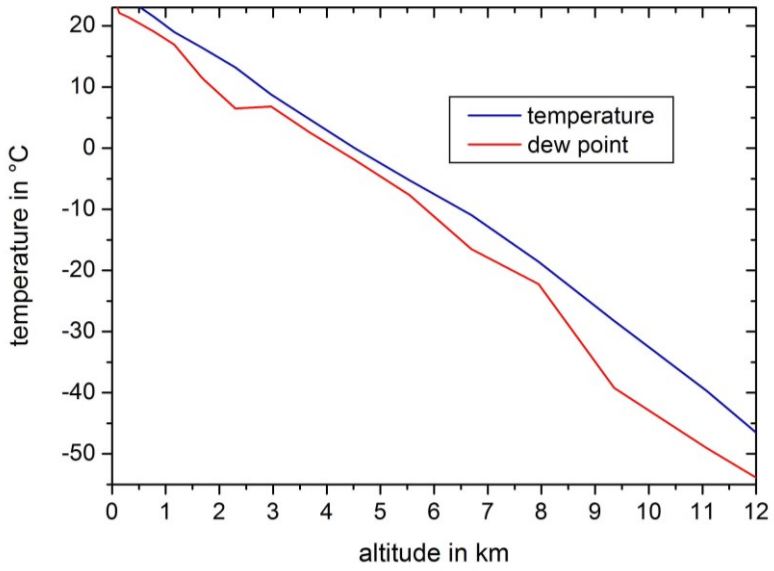

Figure 7: Development of temperature and dew point with altitude during simulations with the air parcel model (Langmann, 2004, pers. comm.).

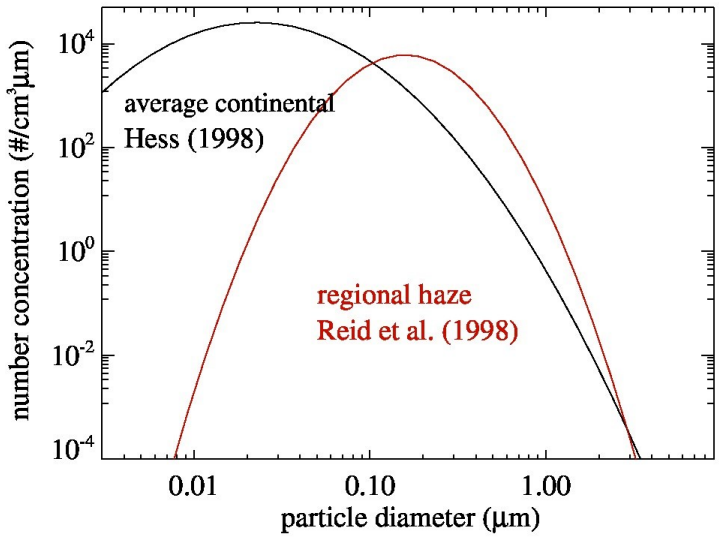

Figure 8: Initial dry aerosol particle number size distributions: Number concentrations per cm^3 and µm as a function of particle diameter.

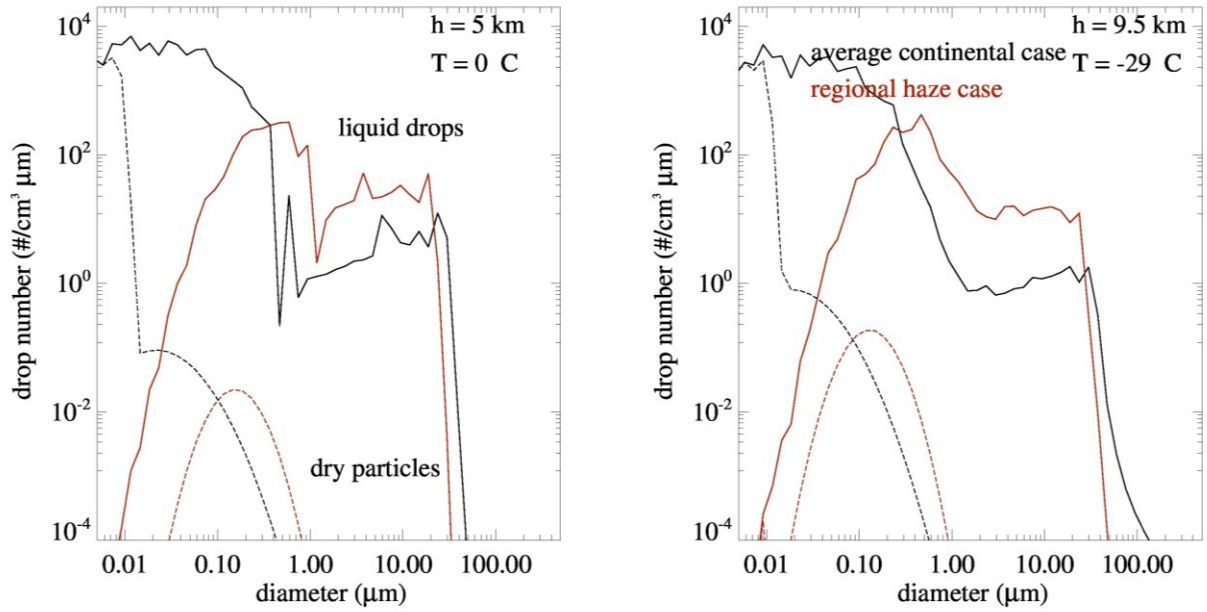

Figure 9: Results from model runs without freezing. Development of liquid drop (solid lines) and interstitial particle numbers (dashed lines) with altitude for two initial aerosol particle number size distributions, average continental (black lines), regional haze (red lines), with ΔT = 2K. Number concentrations per cm^3 and µm as a function of particle diameter.

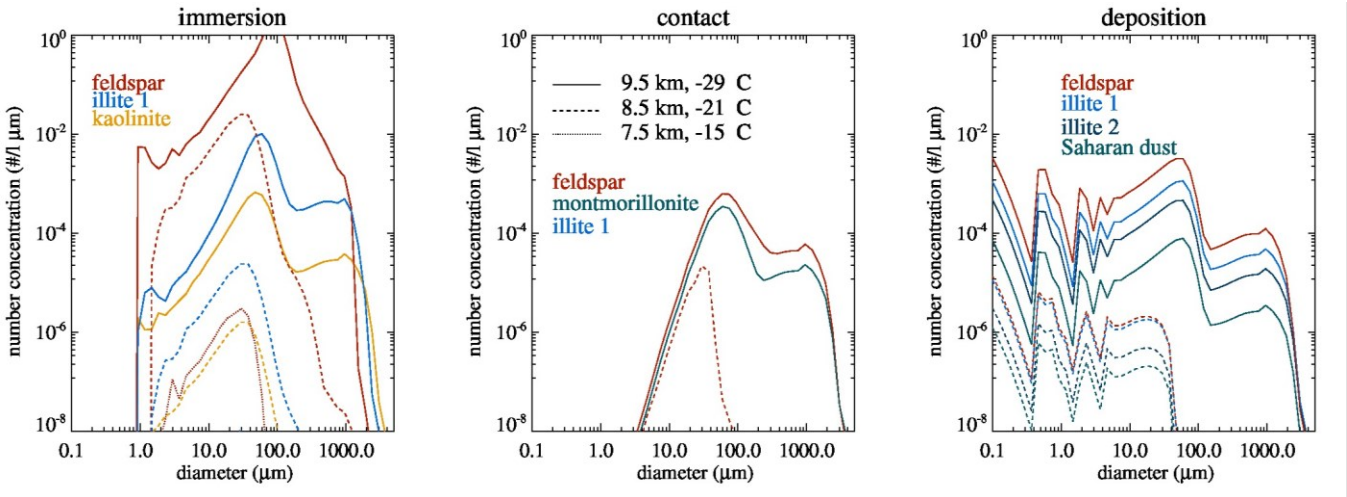

Figure 10: Development of ice particle numbers with altitude and corresponding temperature, marked by different line styles, for deposition, contact and immersion freezing. Types of INP marked by colors. Model simulations with average continental number size distribution and with ΔT = 2K. Number concentrations per l and µm as a function of particle diameter.

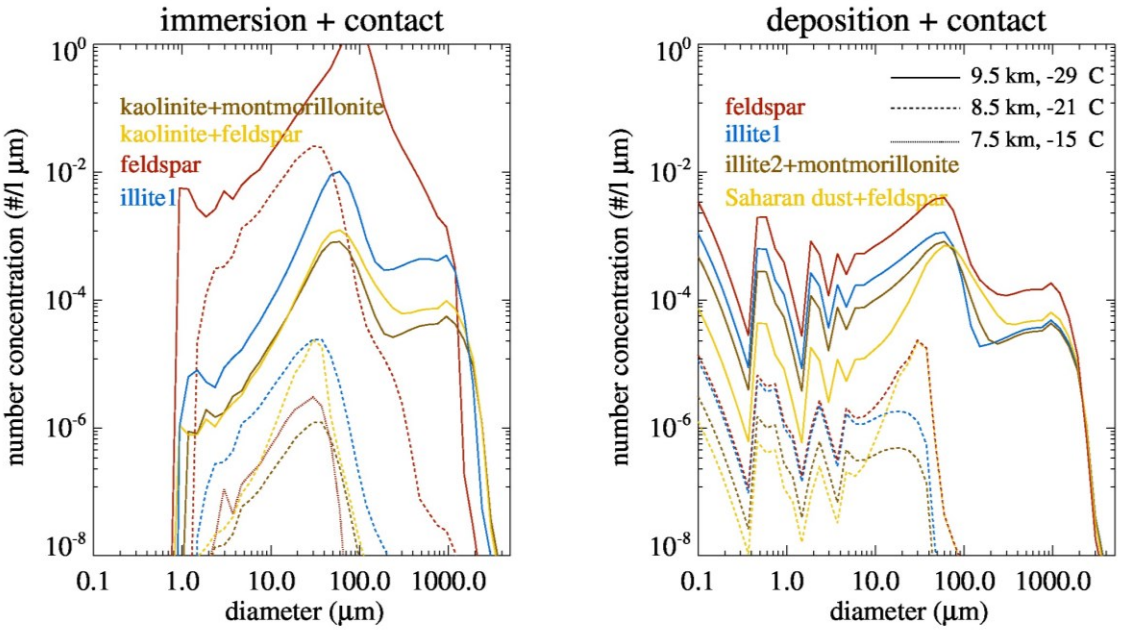

Figure 11: Development of ice particle numbers with altitude and corresponding temperature, marked by different line styles, for coupled freezing processes. Types of INP marked by colors. Model simulations with average continental number size distribution, and with ΔT = 2K. Number concentrations per l and µm as a function of particle diameter.

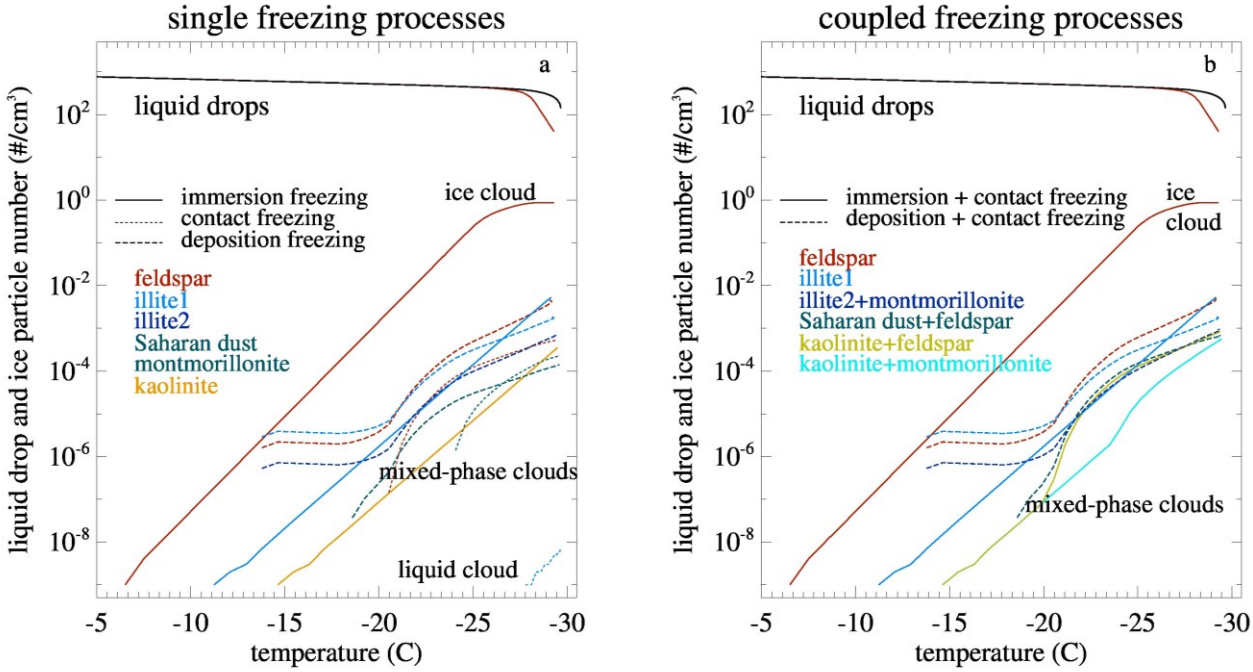

Figure 12: Total numbers of liquid drops and ice particles as a function of temperature for single and coupled freezing processes which are marked by different line styles. Types of INP marked by colors. Model simulations with average continental number size distribution and with ΔT = 2K. Numbers concentrations per cm^3 as a function of temperature.